HANDOUT FOR THE LECTURES ON

"LARGE DEVIATIONS IN RANDOM MATRIX THEORY AND COULOMB GAS SYSTEMS"

BY P. VIVO

A COLLECTION OF REPRINTED PAPERS/FRONTPAGES I WILL REFER TO DURING MY LECTURES.

Numerical Methods for Eigenvalue Distributions of Random Matrices

Alan Edelman and Per-Olof Persson

September 7, 2018

Abstract

We present efficient numerical techniques for calculation of eigenvalue distributions of random matrices in the beta-ensembles. We compute histograms using direct simulations on very large matrices, by using tridiagonal matrices with appropriate simplifications. The distributions are also obtained by numerical solution of the Painlevé II and V equations with high accuracy. For the spacings we show a technique based on the Prolate matrix and Richardson extrapolation, and we compare the distributions with the zeros of the Riemann zeta function.

1 Largest Eigenvalue Distributions

In this section, the distributions of the largest eigenvalue of matrices in the β-ensembles are studied. Histograms are created first by simulation, then by solving the Painlevé II nonlinear differential equation.

1.1 Simulation

The *Gaussian Unitary Ensemble* (GUE) is defined as the Hermitian $n \times n$ matrices A, where the diagonal elements x_{jj} and the upper triangular elements $x_{jk} = u_{jk} + iv_{jk}$ are independent Gaussians with zero-mean, and

$$\begin{cases} \mathrm{Var}(x_{jj}) = 1, & 1 \le j \le n, \\ \mathrm{Var}(u_{jk}) = \mathrm{Var}(v_{jk}) = \frac{1}{2}, & 1 \le j < k \le n. \end{cases} \tag{1}$$

Since a sum of Gaussians is a new Gaussian, an instance of these matrices can be created conveniently in MATLAB:

```
A=randn(n)+i*randn(n);
A=(A+A')/2;
```

The largest eigenvalue of this matrix is about $2\sqrt{n}$. To get a distribution that converges as $n \to \infty$, the shifted and scaled largest eigenvalue $\lambda'_{\max}$ is calculated as

$$\lambda'_{\max} = n^{\frac{1}{6}} \left(\lambda_{\max} - 2\sqrt{n} \right). \tag{2}$$

It is now straight-forward to compute the distribution for $\lambda'_{\max}$ by simulation:

```
for ii=1:trials
  A=randn(n)+i*randn(n);
  A=(A+A')/2;
  lmax=max(eig(A));
  lmaxscaled=n^(1/6)*(lmax-2*sqrt(n));
  % Store lmax
end

% Create and plot histogram
```

The problem with this technique is that the computational requirements and the memory requirements grow fast with n, which should be as large as possible in order to be a good approximation of infinity. Just storing the matrix A requires n^2 double-precision numbers, so on most computers today n has to be less than 10^4. Furthermore, computing all the eigenvalues of a full Hermitian matrix requires a computing time proportional to n^3. This means that it will take many days to create a smooth histogram by simulation, even for relatively small values of n.

To improve upon this situation, another matrix can be studied that has the same eigenvalue distribution as A above. In [2], it was shown that this is true for the following *symmetric* matrix when $\beta = 2$:

$$H_\beta \sim \frac{1}{\sqrt{2}} \begin{pmatrix} N(0,2) & \chi_{(n-1)\beta} & & & & \\ \chi_{(n-1)\beta} & N(0,2) & \chi_{(n-2)\beta} & & & \\ & \ddots & \ddots & \ddots & & \\ & & \chi_{2\beta} & N(0,2) & \chi_\beta & \\ & & & \chi_\beta & N(0,2) \end{pmatrix}. \tag{3}$$

Here, $N(0,2)$ is a zero-mean Gaussian with variance 2, and χ_d is the square-root of a χ^2 distributed number with d degrees of freedom. Note that the

matrix is symmetric, so the subdiagonal and the superdiagonal are always equal.

This matrix has a tridiagonal sparsity structure, and only $2n$ double-precision numbers are required to store an instance of it. The time for computing the largest eigenvalue is proportional to n, either using Krylov subspace based methods or the method of bisection [7].

In MATLAB, the built-in function `eigs` can be used, although that requires dealing with the sparse matrix structure. There is also a large amount of overhead in this function, which results in a relatively poor performance. Instead, the function `maxeig` is used below to compute the eigenvalues. This is not a built-in function in MATLAB, but it can be downloaded from http://www-math.mit.edu/∼persson/mltrid. It is based on the method of bisection, and requires just two ordinary MATLAB vectors as input, corresponding to the diagonal and the subdiagonal.

It also turns out that only the first $10n^{\frac{1}{3}}$ components of the eigenvector corresponding to the largest eigenvalue are significantly greater than zero. Therefore, the upper-left n_{cutoff} by n_{cutoff} submatrix has the same largest eigenvalue (or at least very close), where

$$n_{\text{cutoff}} \approx 10n^{\frac{1}{3}}. \tag{4}$$

Matrices of size $n = 10^{12}$ can then easily be used since the computations can be done on a matrix of size only $10n^{\frac{1}{3}} = 10^5$. Also, for these large values of n the approximation $\chi^2_n \approx n$ is accurate.

A histogram of the distribution for $n = 10^9$ can now be created using the code below.

```
n=1e9;
nrep=1e4;
beta=2;

cutoff=round(10*n^(1/3));
d1=sqrt(n-1:-1:n+1-cutoff)'/2/sqrt(n);

ls=zeros(1,nrep);
for ii=1:nrep
  d0=randn(cutoff,1)/sqrt(n*beta);
  ls(ii)=maxeig(d0,d1);
end

ls=(ls-1)*n^(2/3)*2;

histdistr(ls,-7:0.2:3)
```

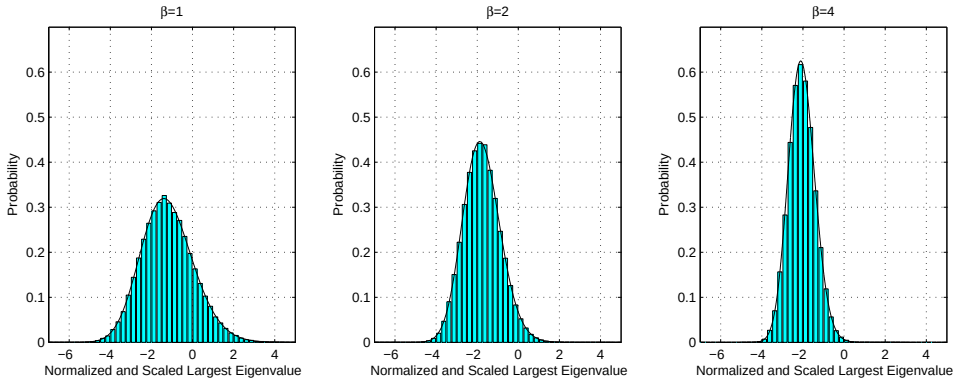

Figure 1: Probability distribution of scaled largest eigenvalue (10^5 repetitions, $n = 10^9$)

where the function `histdistr` below is used to histogram the data. It assumes that the histogram boxes are equidistant.

```
function [xmid,H]=histdistr(ls,x)

dx=x(2)-x(1);
H=histc(ls,x);
H=H(1:end-1);
H=H/sum(H)/dx;
xmid=(x(1:end-1)+x(2:end))/2;

bar(xmid,H)
grid on
```

The resulting distribution is shown in Figure 1, together with distributions for $\beta = 1$ and $\beta = 4$. The plots also contain solid curves representing the "true solutions" (see next section).

1.2 Painlevé II

Instead of using simulation to plot the distributions of the largest eigenvalues, it can be computed from the solution of the Painlevé II nonlinear differential equation [6]:

$$q'' = sq + 2q^3 \tag{5}$$

with the boundary condition

$$q(s) \sim \mathrm{Ai}(s), \qquad \text{as } s \to \infty. \tag{6}$$

The probability distribution $f_2(s)$, corresponding to $\beta = 2$, is then given by

$$f_2(s) = \frac{d}{ds} F_2(s), \tag{7}$$

where

$$F_2(s) = \exp\left(- \int_s^\infty (x - s) q(x)^2 \, dx \right). \tag{8}$$

The distributions for $\beta = 1$ and $\beta = 4$ are the derivatives of

$$F_1(s)^2 = F_2(s) e^{-\int_s^\infty q(x)\, dx} \tag{9}$$

and

$$F_4\left(\frac{s}{2^{\frac{2}{3}}} \right)^2 = F_2(s) \left(\frac{e^{\frac{1}{2}\int_s^\infty q(x)\, dx} + e^{-\frac{1}{2}\int_s^\infty q(x)\, dx}}{2} \right)^2. \tag{10}$$

To solve this numerically using MATLAB, first rewrite (5) as a first-order system:

$$\frac{d}{ds} \begin{pmatrix} q \\ q' \end{pmatrix} = \begin{pmatrix} q' \\ sq + 2q^3 \end{pmatrix}. \tag{11}$$

This can be solved as an initial-value problem starting at $s = s_0 =$ sufficiently large positive number, and integrating along the negative s-axis. The boundary condition (6) then becomes the initial values

$$\begin{cases} q(s_0) &= \mathrm{Ai}(s_0) \\ q'(s_0) &= \mathrm{Ai}'(s_0). \end{cases} \tag{12}$$

Although the distributions can be computed from $q(s)$ as a post-processing step, it is most convenient to add a few variables and equations to the ODE system. When computing $F_2(s)$, the quantity $I(s) = \int_s^\infty (x - s) q(x)^2 \, dx$ is required. Differentiate this twice to get

$$I'(s) = - \int_s^\infty q(x)^2 \, dx \tag{13}$$

and

$$I''(s) = q(s)^2. \tag{14}$$

Add these equations and the variables $I(s), I'(s)$ to the ODE system, and the solver will do the integration. This is not only easier and gives less code, it will also give a much more accurate solution since the same tolerance requirements are imposed on $I(s)$ as on the solution $q(s)$.

In a similar way, the quantity $J(s) = \int_s^\infty q(x)\,dx$ is needed when computing $F_1(s)$ and $F_4(s)$. This is handled by adding the variable $J(s)$ and the equation $J'(s) = -q(s)$.

The final system now has the form

$$\frac{d}{ds}\begin{pmatrix} q \\ q' \\ I \\ I' \\ J \end{pmatrix} = \begin{pmatrix} q' \\ sq + 2q^3 \\ I' \\ q^2 \\ -q \end{pmatrix} \tag{15}$$

with the initial condition

$$\begin{pmatrix} q(s_0) \\ q'(s_0) \\ I(s_0) \\ I'(s_0) \\ J(s_0) \end{pmatrix} = \begin{pmatrix} \mathrm{Ai}(s_0) \\ \mathrm{Ai}'(s_0) \\ \int_{s_0}^\infty (x - s_0)\mathrm{Ai}(x)^2\,dx \\ \mathrm{Ai}(s_0)^2 \\ \int_{s_0}^\infty \mathrm{Ai}(x)\,dx \end{pmatrix}. \tag{16}$$

This problem can be solved in just a few lines of MATLAB code using the built-in Runge-Kutta based ODE solver `ode45`. First define the system of equations as an inline function

```
deq=inline('[y(2); s*y(1)+2*y(1)^3; y(4); y(1)^2; -y(1)]','s','y');
```

Next specify the integration interval and the desired output times.

```
s0=5;
sn=-8;
sspan=linspace(s0,sn,1000);
```

The initial values can be computed as

```
y0=[airy(s0); airy(1,s0); ...
    quadl(inline('(x-s0).*airy(x).^2','x','s0'),s0,20,1e-25,0,s0); ...
    airy(s0)^2; quadl(inline('airy(x)'),s0,20,1e-18)];
```

where the `quadl` function is used to numerically approximate the integrals in (16). Now, the integration tolerances can be set and the system integrated:

```
opts=odeset('reltol',1e-13,'abstol',1e-15);
[s,y]=ode45(deq,sspan,y0,opts);
```

The five dependent variables are now in the columns of the MATLAB variable `y`. Using these, $F_2(s), F_1(s)$, and $F_4(s)$ become

```
F2=exp(-y(:,3));
F1=sqrt(F2.*exp(-y(:,5)));
F4=sqrt(F2).*(exp(y(:,5)/2)+exp(-y(:,5)/2))/2;
s4=s/2^(2/3);
```

The probability distributions $f_2(s), f_1(s)$, and $f_4(s)$ could be computed by numerical differentiation:

```
f2=gradient(F2,s);
f1=gradient(F1,s);
f4=gradient(F4,s4);
```

but it is more accurate to first do the differentiation symbolically:

$$f_2(s) = -I'(s)F_2(s) \tag{17}$$

$$f_1(s) = \frac{1}{2F_1(s)}\left(f_2(s) + q(s)F_2(s)\right)e^{-J(s)} \tag{18}$$

$$f_4(s) = \frac{1}{2^{\frac{1}{3}}4F_4(s)}\left(f_2(s)\left(2 + e^{J(s)} + e^{-J(s)}\right) + F_2(s)q(s)\left(e^{-J(s)} - e^{J(s)}\right)\right) \tag{19}$$

and evaluate these expressions:

```
f2=-y(:,4).*F2;
f1=1/2./F1.*(f2+y(:,1).*F2).*exp(-y(:,5));
f4=1/2^(1/3)/4./F4.*(f2.*(2+exp(y(:,5))+exp(-y(:,5)))+ ...
                     F2.*y(:,1).*(exp(-y(:,5))-exp(y(:,5))));
```

Finally, plot the curves:

```
plot(s,f1,s,f2,s4,f4)
legend('\beta=1','\beta=2','\beta=4')
xlabel('s')
ylabel('f_\beta(s)','rotation',0)
grid on
```

The result can be seen in Figure 2.

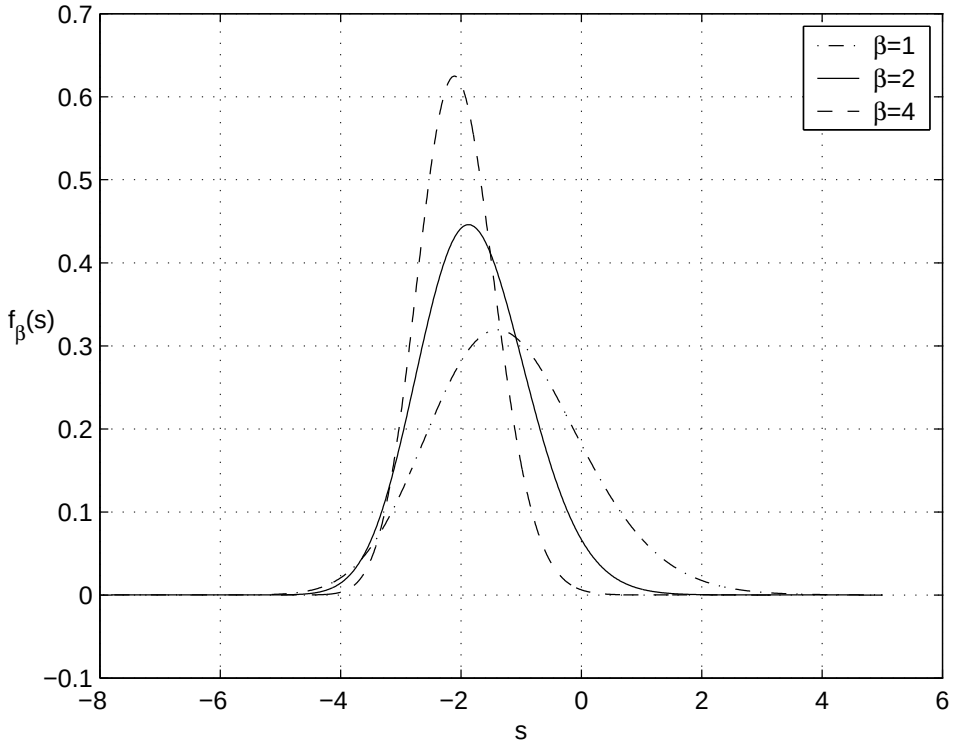

Figure 2: The probability distributions $f_1(s)$, $f_2(s)$, and $f_4(s)$, computed using the Painlevé II solution.

2 Eigenvalue Spacings Distributions

Another quantity with an interesting probability distribution is the spacings of the eigenvalues of random matrices. It turns out that the eigenvalues are almost uniformly distributed, which means that every random matrix gives a large number of spacings. The distributions can then be efficiently computed by simulation.

Two other methods are used to compute the spacings distribution – the solution of the Painlevé V nonlinear differential equation and the eigenvalues of the Prolate matrix. Finally, the results are compared with the spacings of the zeros along the critical line of the Riemann zeta function.

2.1 Simulation

As before, the simulations are made with matrices from the Gaussian Unitary Ensemble. The normalized spacings of the eigenvalues $\lambda_1 \leq \lambda_2 \leq \ldots \leq \lambda_N$ are computed according to

$$\delta'_k = \frac{\lambda_{k+1} - \lambda_k}{\pi\beta}\sqrt{2\beta n - \lambda_k^2}, \qquad k \approx n/2, \tag{20}$$

where $\beta = 2$ for the GUE. The distribution of the eigenvalues is almost uniform, with a slight deviation at the two ends of the spectrum. Therefore, only half of the eigenvalues are used, and one quarter of the eigenvalues at each end is discarded.

Again, to allow for a more efficient simulation, the tridiagonal matrix (3) is used instead of the full Hermitian matrix. In this case, all the eigenvalues are computed, which can be done in a time proportional to n^2. While this could in principle be done using the MATLAB sparse matrix structure and the `eigs` function, the more efficient `trideig` function is used below to compute all the eigenvalues of a symmetric tridiagonal matrix. It can be downloaded from http://www-math.mit.edu/∼persson/mltrid.

The histogram can now be computed by simulation with the following lines of code. Note that the function `chi2rnd` from the Statistics Toolbox is required.

```
n=1000;
nrep=1000;
beta=2;

ds=zeros(1,nrep*n/2);
for ii=1:nrep
  l=trideig(randn(n,1),sqrt(chi2rnd((n-1:-1:1)'*beta)/2));
```

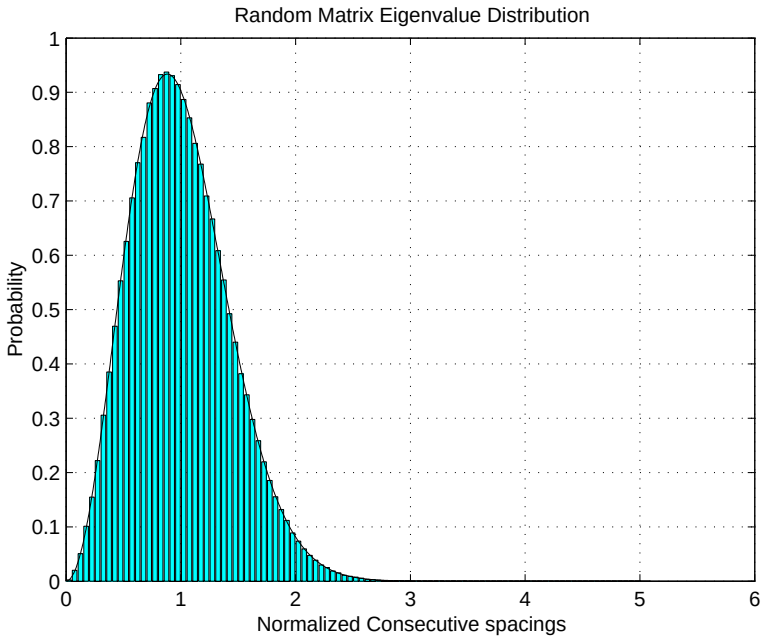

Figure 3: Probability distribution of consecutive spacings of random matrix eigenvalues (1000 repetitions, $n = 1000$)

```
  d=diff(l(n/4:3*n/4))/beta/pi.*sqrt(2*beta*n-l(n/4:3*n/4-1).^2);
  ds((ii-1)*n/2+1:ii*n/2)=d;
end

histdistr(ds,0:0.05:5);
```

The resulting histogram can be found in Figure 3. The figure also shows the expected curve as a solid line.

2.2 Painlevé V

The probability distribution $p(s)$ for the eigenvalue spacings when $\beta = 2$ can be computed with the solution to the Painlevé V nonlinear differential equation (see [5] for details):

$$(t\sigma'')^2 + 4(t\sigma' - \sigma)\left(t\sigma' - \sigma + (\sigma')^2\right) = 0 \tag{21}$$

with the boundary condition

$$\sigma(t) \approx -\frac{t}{\pi} - \left(\frac{t}{\pi}\right)^2, \qquad \text{as } t \to 0^+. \tag{22}$$

Then $p(s)$ is given by

$$p(s) = \frac{d^2}{ds^2} E(s) \tag{23}$$

where

$$E(s) = \exp\left(\int_0^{\pi s} \frac{\sigma(t)}{t} dt\right). \tag{24}$$

Explicit differentiation gives

$$p(s) = \frac{1}{s^2}\left(\pi s \sigma'(\pi s) - \sigma(\pi s) + \sigma(\pi s)^2\right) E(s). \tag{25}$$

The second-order differential equation (21) can be written as a first-order system of differential equations:

$$\frac{d}{dt}\begin{pmatrix}\sigma \\ \sigma'\end{pmatrix} = \begin{pmatrix}\sigma' \\ -\frac{2}{t}\sqrt{(\sigma - t\sigma')\left(t\sigma' - \sigma + (\sigma')^2\right)}\end{pmatrix}. \tag{26}$$

This is solved as an initial-value problem starting at $t = t_0 =$ very small positive number. The value $t = 0$ has to be avoided because of the division by t in the system of equations. This is not a problem, since the boundary condition (22) provides an accurate value for $\sigma(t_0)$ (as well as $E(t_0/\pi)$). The boundary conditions for the system (26) then become

$$\begin{cases}\sigma(t_0) & = -\frac{t_0}{\pi} - \left(\frac{t_0}{\pi}\right)^2 \\ \sigma'(t_0) & = -\frac{1}{\pi} - \frac{2t_0}{\pi}.\end{cases} \tag{27}$$

To be able to compute $E(s)$ using (24), the variable

$$I(t) = \int_0^t \frac{\sigma(t')}{t'}\, dt' \tag{28}$$

is added to the system, as well as the equation $\frac{d}{dt} I = \frac{\sigma}{t}$. The corresponding initial value is

$$I(t_0) \approx \int_0^{t_0} \left(-\frac{1}{\pi} - \frac{t}{\pi^2}\right) dt = -\frac{t_0}{\pi} - \frac{t_0^2}{2\pi^2}. \tag{29}$$

Putting it all together, the final system is

$$\frac{d}{dt}\begin{pmatrix}\sigma\\ \sigma'\\ I\end{pmatrix} = \begin{pmatrix}\sigma'\\ -\frac{2}{t}\sqrt{(\sigma - t\sigma')\left(t\sigma' - \sigma + (\sigma')^2\right)}\\ \frac{\sigma}{t}\end{pmatrix} \tag{30}$$

with boundary condition

$$\begin{pmatrix}\sigma(t_0)\\ \sigma'(t_0)\\ I(t_0)\end{pmatrix} = \begin{pmatrix}-\frac{t_0}{\pi} - \left(\frac{t_0}{\pi}\right)^2\\ -\frac{1}{\pi} - \frac{2t_0}{\pi}\\ -\frac{t_0}{\pi} - \frac{t_0^2}{2\pi^2}\end{pmatrix}. \tag{31}$$

This system is defined as an inline function in MATLAB:

```
desig=inline(['[y(2); -2/t*sqrt((y(1)-t*y(2))*' ...
              '(t*y(2)-y(1)+y(2)^2)); y(1)/t]'],'t','y');
```

Specify the integration interval and the desired output times:

```
t0=1e-12;
tn=16;
tspan=linspace(t0,tn,1000);
```

Set the initial condition:

```
y0=[-t0/pi-(t0/pi)^2; -1/pi-2*t0/pi; -t0/pi-t0^2/2/pi^2];
```

Finally, set the integration tolerances and call the solver:

```
opts=odeset('reltol',1e-13,'abstol',1e-14);
[t,y]=ode45(desig,tspan,y0,opts);
```

The solution components are now in the columns of `y`. Use these to evaluate $E(s)$ and $p(s)$:

```
s=t/pi;
E=exp(y(:,3));
p=1./s.^2.*E.*(t.*y(:,2)-y(:,1)+y(:,1).^2);
p(1)=2*s(1); % Fix due to cancellation
```

A plot of $p(s)$ can be made with the command

```
plot(s,p)
grid on
```

and it can be seen in Figure 4. Plots are also shown of $E(s)$ and $\sigma(t)$.

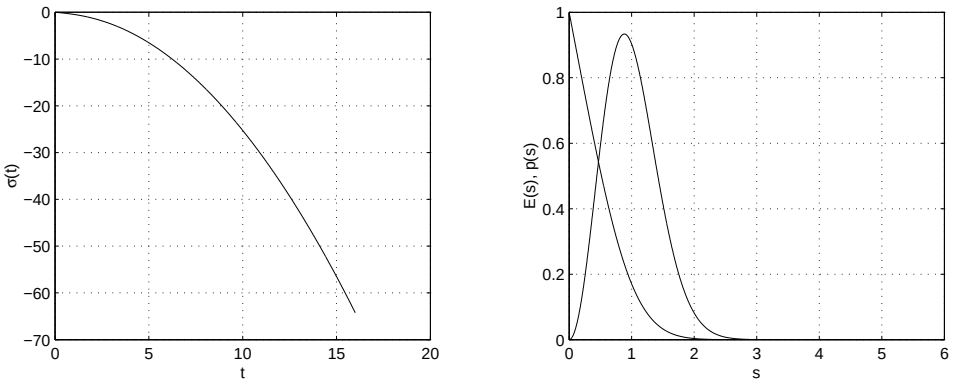

Figure 4: Painlevé V (left), $E(s)$ and $p(s)$ (right).

2.3 The Prolate Matrix

Another method to calculate the distribution of the eigenvalue spacings is to compute the eigenvalues λ_i of the operator

$$f(y) \to \int_{-1}^{1} Q(x,y) f(y)\, dy, \qquad Q(x,y) = \frac{\sin\left((x-y)\pi t\right)}{(x-y)\pi}. \tag{32}$$

Then $E(2t) = \prod_i (1-\lambda_i)$, and $p(s)$ can be computed as before. To do this, first define the infinite symmetric Prolate matrix:

$$A_\infty = \begin{pmatrix} a_0 & a_1 & \dots \\ a_1 & a_0 & \dots \\ \vdots & \vdots & \ddots \end{pmatrix} \tag{33}$$

with $a_0 = 2w$, $a_k = (\sin 2\pi w k)/\pi k$ for $k = 1, 2, \dots$, and $0 < w < \frac{1}{2}$. A discretization of $Q(x,y)$ is achieved by setting $w = t/n$ and extracting the upper-left $n \times n$ submatrix A_n of A_∞.

Below, the full matrix A_n is used, and all the eigenvalues are computed in n^3 time using the `eig` function. However, A_n commutes with the following symmetric tridiagonal matrix [4], and therefore has the same eigenvectors:

$$T_n = \begin{pmatrix} \alpha_1 & \beta_1 & & & \\ \beta_1 & \alpha_2 & \beta_2 & & \\ & \ddots & \ddots & \ddots & \\ & & \beta_{n-2} & \alpha_{n-1} & \beta_{n-1} \\ & & & \beta_{n-1} & \alpha_n \end{pmatrix} \tag{34}$$

where

$$\left\{ \begin{array}{rcl} \alpha_k & = & \left(\frac{n+1}{2} - k\right)^2 \cos 2\pi w \\ \beta_k & = & \frac{1}{2}k(n-k). \end{array} \right. \tag{35}$$

It is then in principle possible to use the new techniques described in [1] to compute all the eigenvalues and eigenvectors of T_n in n^2 time, and then get the eigenvalues of A_n by dot products. This is not done in this example.

The code for computing $E(s)$ is shown below. This time, $p(s)$ is evaluated by numerical differentiation since no information about the derivative of $E(s)$ is available.

```
s=0:0.01:5;
n=100;
E0=zeros(size(s));
for ii=1:length(s)
  Q=gallery('prolate',n,s(ii)/2/n);
  E0(ii)=prod(1-eig(Q));
end
p0=gradient(gradient(E0,s),s);
```

To improve the accuracy in $E(s)$, Richardson extrapolation can be used. This is done as follows, where the values are assumed to converge as $1/n^2$:

```
% ... Compute s and E using Painleve V in previous section

Es=zeros(length(t),0);
E1=zeros(size(s));
for n=20*2.^(0:3)
  for ii=1:length(s)
    Q=gallery('prolate',n,s(ii)/2/n);
    E1(ii)=prod(1-eig(Q));
  end
  Es=[Es,E1];
end

for ii=1:3
  max(abs(Es-E(:,ones(1,size(Es,2)))))
  Es=Es(:,2:end)+diff(Es,1,2)/(2^(ii+1)-1);
end
max(abs(Es-E))
```

The errors $\max_{0\le s\le 5} |E_1(s) - E(s)|$ are shown in Table 1, for $n = 20, 40, 80,$ and 160. The error after all extrapolations is of the same order as the "exact solution" using Painlevé V.

N	Error 0	Error 1	Error 2	Error 3
20	0.2244			
40	0.0561	0.7701		
80	0.0140	0.0483	0.5486	
160	0.0035	0.0032	0.0323	2.2673
	$\cdot 10^{-3}$	$\cdot 10^{-7}$	$\cdot 10^{-8}$	$\cdot 10^{-11}$

Table 1: Difference between Prolate solution $E_1(s)$ and Painlevé V solution $E(s)$ after 0, 1, 2, and 3 Richardson extrapolations.

2.4 Riemann Zeta Zeros

It has been observed that the zeros of the Riemann zeta function along the critical line $\mathrm{Re}(z) = \frac{1}{2}$ behave similar to the eigenvalues of random matrices in the GUE. Here, the distribution of the scaled spacings of the zeros is compared to the corresponding distribution for eigenvalues computed using the Painlevé V equation from the previous chapters.

Define the nth zero $\gamma_n = n^{\text{th}}$ as

$$\zeta\left(\frac{1}{2} + i\gamma_n\right) = 0, \qquad 0 < \gamma_1 < \gamma_2 < \dots \tag{36}$$

Compute a normalized spacing:

$$\tilde{\gamma}_n = \frac{\gamma_n}{\text{av spacing near } \gamma_n} = \gamma_n \cdot \left[\frac{\log \gamma_n/2\pi}{2\pi}\right]. \tag{37}$$

Zeros of the Riemann zeta function can be downloaded from [3]. Assuming that the MATLAB variable `gamma` contains the zeros, and the variable `offset` the offset, these two lines compute the consecutive spacings $\tilde{\gamma}_{n+1} - \tilde{\gamma}_n$ and plot the histogram:

```
delta=diff(gamma)/2/pi.*log((gamma(1:end-1)+offset)/2/pi);
histdistr(delta,0:0.05:5.0);
```

The result can be found in Figure 5, along with the Painlevé V distribution. The curves are indeed in good agreement, although the number of samples here is a little to low to get a perfect match.

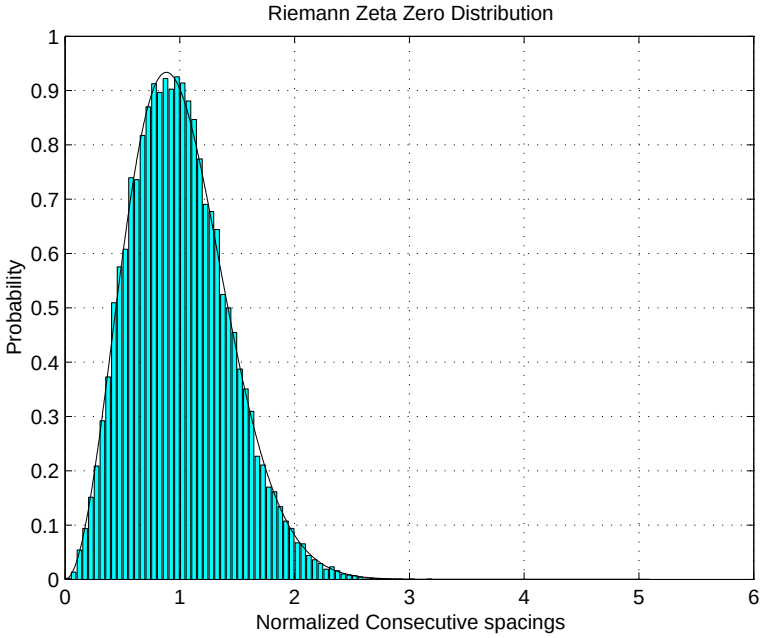

Figure 5: Probability distribution of consecutive spacings of Riemann zeta zeros ($30,000$ zeros, $n \approx 10^{12}, 10^{21}, 10^{22}$)

References

[1] Inderjit S. Dhillon. *A new $\mathcal{O}(N^2)$ algorithm for the symmetric tridiagonal eigenvalue/eigenvector problem*. PhD thesis, University of California, Berkeley, 1997.

[2] Ioana Dumitriu and Alan Edelman. Matrix models for beta ensembles. *J. Math. Phys.*, 43(11):5830–5847, 2002.

[3] Andrew Odlyzko. Tables of zeros of the riemann zeta function. http://www.dtc.umn.edu/∼odlyzko/zeta_tables/index.html.

[4] David Slepian. Prolate spheroidal wave functions, Fourier analysis and uncertainity. IV. Extensions to many dimensions; generalized prolate spheroidal functions. *Bell System Tech. J.*, 43:3009–3057, 1964.

[5] Craig A. Tracy and Harold Widom. Introduction to random matrices. In *Geometric and quantum aspects of integrable systems (Scheveningen, 1992)*, volume 424 of *Lecture Notes in Phys.*, pages 103–130. Springer, Berlin, 1993.

[6] Craig A. Tracy and Harold Widom. The distribution of the largest eigenvalue in the Gaussian ensembles: $\beta = 1, 2, 4$. In *Calogero-Moser-Sutherland models (Montréal, QC, 1997)*, CRM Ser. Math. Phys., pages 461–472. Springer, New York, 2000.

[7] Lloyd N. Trefethen and David Bau, III. *Numerical linear algebra*. Society for Industrial and Applied Mathematics (SIAM), Philadelphia, PA, 1997.

ON THE DISTRIBUTION OF ROOTS OF CERTAIN DETERMINANTAL EQUATIONS

By P. L. HSU

THE extension (Fisher, 1938) of Fisher's discriminant analysis to more than two multivariate samples has directed attention to the problem of the exact distribution of the roots of a certain type of determinantal equation, which are required for various significance tests. While Fisher was solving this problem he submitted it to me for its interest in relation to matrix algebra. The purpose of the present paper is to give a complete demonstration of the analytic solution, including the case in which the number of variates, p, exceeds one of the sample numbers n_1.

Consider a set of $p(n_1+n_2)$ random variables

$$y_{ir},\ z_{it} \quad (i = 1, 2, \ldots, p;\ r = 1, 2, \ldots, n_1;\ t = 1, 2, \ldots, n_2),$$

following the distribution law

$$\text{const. } \exp\left[-\tfrac{1}{2}\sum_{i,j=1}^{p}\alpha_{ij}(a_{ij}+b_{ij})\right]\prod dy\,dz, \qquad \ldots\ldots(1)$$

where

$$a_{ij} = \sum_{r=1}^{n_1} y_{ir}y_{jr}, \quad b_{ij} = \sum_{t=1}^{n_2} z_{it}z_{jt}.$$

We shall assume that $n_2 \geqslant p$, so that the matrix $\|b_{ij}\|$ is almost always positively definite. Thus the determinantal equation

$$|a_{ij}-\theta(a_{ij}+b_{ij})| = 0 \qquad \ldots\ldots(2)$$

is known to possess exactly p or n_1 (whichever is smaller) real, not identically vanishing, roots, each lying between 0 and 1. Denoting them by $\theta_1, \theta_2, \ldots$, in the order of descending magnitude, we shall now establish the simultaneous distribution of these θ's.

THEOREM 1. *The simultaneous distribution of the roots of* (2) *is given by*

$$CP\left\{\prod_{i=1}^{p}\theta_i\right\}^{\frac{1}{2}(n_1-p-1)}\left\{\prod_{i=1}^{p}(1-\theta_i)\right\}^{\frac{1}{2}(n_2-p-1)}\prod_{i=1}^{p}d\theta_i, \text{ if } p \leqslant n_1, \qquad \ldots\ldots(3)$$

and

$$C_1P_1\left\{\prod_{i=1}^{n_1}\theta_i\right\}^{\frac{1}{2}(p-n_1-1)}\left\{\prod_{i=1}^{n_1}(1-\theta_i)\right\}^{\frac{1}{2}(n_2-p-1)}\prod_{i=1}^{n_1}d\theta_i, \text{ if } n_1 \leqslant p, \qquad \ldots\ldots(4)$$

where

$$C = \pi^{\frac{1}{2}p}\prod_{i=1}^{p}\frac{\Gamma\frac{1}{2}(n_1+n_2-i+1)}{\Gamma\frac{1}{2}(n_1-i+1)\,\Gamma\frac{1}{2}(n_2-i+1)\,\Gamma\frac{1}{2}(p-i+1)},$$

$$C_1 = \pi^{\frac{1}{2}n_1}\prod_{i=1}^{n_1}\frac{\Gamma\frac{1}{2}(n_1+n_2-i+1)}{\Gamma\frac{1}{2}(n_1-i+1)\,\Gamma\frac{1}{2}(n_1+n_2-p-i+1)\,\Gamma\frac{1}{2}(p-i+1)},$$

and

$$P = \prod_{i=1}^{p}\prod_{j=i+1}^{p}(\theta_i-\theta_j), \quad P_1 = \prod_{i=1}^{n_1}\prod_{j=i+1}^{n_1}(\theta_i-\theta_j).$$

Theorem 2. *If the* $\frac{1}{2}p(p+1)$ *variables* $s_{ij}(i \leqslant j = 1, 2, \ldots, p)$ *have such a domain of existence that the symmetric matrix* $\| s_{ij} \|$ *is always non-singular, and if they are so distributed that their joint probability density function depends only on the latent roots, say* $\lambda_1, \lambda_2, \ldots, \lambda_p$, *arranged in the order of descending magnitude, of* $\| s_{ij} \|$, *i.e. if*

$$df = g(\lambda_1, \lambda_2, \ldots, \lambda_p) \prod ds_{ij},$$

then the joint distribution law of the λ_i *is the following:*

$$\pi^{\frac{1}{4}p(p+1)} \left\{ \prod_{i=1}^{p} \Gamma\tfrac{1}{2}(p-i+1) \right\}^{-1} \left\{ \prod_{i=1}^{p} \prod_{j=i+1}^{p} (\lambda_i - \lambda_j) \right\} g(\lambda_1, \ldots, \lambda_p) \prod d\lambda. \quad \ldots\ldots(24)$$

Proof. It is a familiar argument that the general formula (24) will follow if we can find a particular example for g for which (24) holds true. This is because the multiplier of g in (24) is entirely independent of the function g itself. The required example is found in the proof of Theorem 1.

Let us take the case $n_1 \geqslant p$ in the distribution law (18). We have seen that the roots of (17) follow the distribution (3). Writing

$$s_{ij} = \sum_{r=1}^{n_1} u_{ir} u_{jr},$$

we get, as a consequence of Wishart's formula, the following distribution for the s_{ij}:

$$C_6 \,|\, s_{ij} \,|^{\frac{1}{2}(n_1-p-1)} \,|\, \delta_{ij} - s_{ij} \,|^{\frac{1}{2}(n_2-p-1)} \prod ds, \quad \ldots\ldots(25)$$

where $\delta_{ii} = 1$ and $\delta_{ij} = 0$ for $i \neq j$, and

$$C_6 = \pi^{-\frac{1}{4}p(p-1)} \prod_{i=1}^{p} \frac{\Gamma\tfrac{1}{2}(n_1+n_2-i+1)}{\Gamma\tfrac{1}{2}(n_1-i+1)\,\Gamma\tfrac{1}{2}(n_2-i+1)}.$$

Now the probability density function appearing in (25) depends on the latent roots of $\| s_{ij} \|$ only. It is in fact equal to

$$C_6 \left\{ \prod_{i=1}^{p} \lambda_i \right\}^{\frac{1}{2}(n_1-p-1)} \left\{ \prod_{i=1}^{p} (1-\lambda_i) \right\}^{\frac{1}{2}(n_2-p-1)}. \quad \ldots\ldots(26)$$

On the other hand, the λ_i follow the distribution (3), with the replacement of θ by λ. In other words, the probability density function of the λ_i is (26) multiplied by the expression which coincides with the multiplier of g in (24). Thus Theorem 2 is proved.

As an application of Theorem 2 let us take the following example. Suppose that the pn random variables y_{ir} $(i = 1, 2, \ldots, p;\ r = 1, 2, \ldots, n)$ follow the distribution

$$\text{const. } \exp\left[-\tfrac{1}{2} \sum_{i,j=1}^{p} \alpha_{ij} s_{ij} \right] \prod dy,$$

where

$$s_{ij} = \sum_{r=1}^{p} y_{ir} y_{jr}.$$

The fact that $S(x)$ is differentiable and that, therefore, the first integral can be replaced by the second one ($\sigma(x) = S'(x)$) will be a consequence of (17). From the vanishing of the odd moments $M_{2\nu+1}$ it follows that $\sigma(x)$ is an even function of x. The form of the even moments suggests the introduction of new variables

$$\rho(\xi) = N\sigma(N\xi) \tag{18}$$

in terms of which (17) reads

$$\int \xi^{2\nu}\rho(\xi)\,d\xi = \frac{(2\nu)!\,2^\nu}{\nu!(\nu+1)!}\frac{v^{2\nu}}{N^\nu} = \frac{(2\nu)!(2q)^\nu}{\nu!(\nu+1)!} \tag{18a}$$

where $q = v^2/N$.

Professor W. Feller kindly pointed out to the writer that the analysis of the original manuscript leading to (20) can be simplified by calculating directly (cf. also [2], Chapters 14 and 16),

$$\begin{aligned}\int e^{ik\xi}\rho(\xi)\,d\xi &= \sum_{\nu=0}^{\infty}\int \frac{(ik\xi)^{2\nu}}{(2\nu)!}\rho(\xi)\,d\xi \\ &= \sum_\nu \frac{(-)^\nu(2qk^2)^\nu}{\nu!(\nu+1)!} = \frac{2J_1(q'k)}{q'k}\end{aligned} \tag{19}$$

where $q' = (8q)^{\frac{1}{2}}$. The second member of (19) follows from the vanishing of the odd moments, the third member is the well known series (see [5], 17.1, p. 355) for the Bessel function of order 1. In order to obtain ρ itself, the Bessel function must be represented as a Fourier integral. Such a representation is provided by the expression (see [5], Example 1, p. 366),

$$\begin{aligned}J_1(z) &= \frac{\frac{1}{2}z}{\Gamma(3/2)\Gamma(1/2)}\int_0^\pi e^{iz\cos\varphi}\sin^2\varphi\,d\varphi \\ &= \frac{z}{\pi}\int_{-1}^{1} e^{izw}(1-w^2)^{\frac{1}{2}}\,dw.\end{aligned} \tag{19a}$$

The last part was obtained by substituting w for $\cos\varphi$. Substitution of $q'k$ for z and ξ for $q'w$ then gives (remembering that $q'^2 = 8q$)

$$\frac{2J_1(q'k)}{q'k} = \frac{1}{4\pi q}\int_{-q'}^{q'} e^{ik\xi}(8q-\xi^2)^{\frac{1}{2}}\,d\xi. \tag{19b}$$

Comparison of (19b) with (19) yields

$$\begin{aligned}\rho(\xi) &= (4\pi q)^{-1}(8q-\xi^2)^{\frac{1}{2}} && \text{for } \xi^2 < 8q \\ &= 0 && \text{elsewhere.}\end{aligned} \tag{20}$$

The original analysis did not make use of the properties of Bessel functions. It showed, on the basis of (18a), that the moments of $(8q/\xi)\,ds/d\xi$ and of $\xi\,ds/d\xi - 3s$ are equal where $ds/d\xi = \xi\rho$. This led to the differential equation

$$(8q/\xi)\,ds/d\xi = \xi\,ds/d\xi - 3s \tag{19c}$$

$$(5)\quad P(\lambda_1, \lambda_2, \ldots, \lambda_n) = \text{const} \prod_{i<k} |\lambda_i - \lambda_k| \exp[-\tfrac{1}{4} \sum \lambda_i^2].$$

One might conclude that it is easy to calculate, from (5), not only the number of characteristic values in unit interval at λ:

$$(5a)\quad \sigma(\lambda) = n \int_{-\infty}^{\infty} \ldots \int P(\lambda, \lambda_2, \ldots, \lambda_n)\, d\lambda_2 \ldots d\lambda_n$$

but also the distribution of the intervals between adjacent roots. The latter could be done by integrating (5) over all but *two* of the λ. However, even the integration (5a), over the very simple domain indicated, is prohibitively difficult if n is a large number. It is necessary, therefore, to use less direct methods to obtain the quantities of interest. This was done by Bargmann and Von Neumann who obtained expressions for the distribution of the smallest, and of the largest, characteristic value.[1]

In order to calculate the over-all density $\sigma(\lambda)$ of the characteristic values, one may observe that the problem is, mathematically, very similar to problems encountered in statistical mechanics. One may use, therefore, the approximate methods of that discipline. If the density of the roots at λ is $\sigma(\lambda)$, the logarithm of the probability P is given by

$$(6)\quad \ln P(\lambda_1, \lambda_2, \ldots, \lambda_n) = \text{const} - \sum_i \tfrac{1}{4}\lambda_i^2 + \sum_{i<k} \ln|\lambda_i - \lambda_k|.$$

It can be approximated by the following functional of σ

$$(6a)\quad [\sigma] = \text{const} - \tfrac{1}{4}\int d\lambda\, \lambda^2\sigma(\lambda) + \tfrac{1}{2}\int d\lambda \int d\mu \sigma(\lambda)\sigma(\mu) \ln|\lambda - \mu|.$$

All integrations have to be extended from $-\infty$ to ∞ and σ is so normalized that

$$(7)\quad \int \sigma(\lambda) d\lambda = n.$$

The first integral in (6a) reproduces the first sum of (6) accurately if the number of dimensions n is sufficiently high. This is not true

[1]Personal communication of Dr. V. Bargmann. The smallest and largest characteristic values of the matrices of the Wishart set lie in the energy regions in which the density of the energy levels tends to zero as n increases. Hence, $\sigma(\lambda) = 0$ for both lowest and highest roots considered by Bargmann and Von Neumann. See also H. H. Goldstine and J. V. Neumann, Bull. Amer. Math. Soc., *53* (1947), 1021, and particularly Proc. Amer. Math. Soc., *2* (1951), 188.

of the second integral: this neglects correlations between the positions of the roots. However, these correlations can be expected to extend only over a few neighbouring roots and since the total number of roots is large and since the second integral in (6a) converges, one can expect that the effect of the correlations between the positions of the roots is negligible. The factor $\frac{1}{2}$ of the second integral in (6a) stems from the condition $i < k$ in (6).

One may now proceed, as in statistical mechanics, by postulating that the actual density makes the expression $[\sigma]$ a maximum consistent with the requirement (7) and the condition $\sigma(\lambda) \geqslant 0$. This leads to the integral equation

$$-\tfrac{1}{4}\lambda^2 + \int d\mu\, \sigma(\mu) \ln|\lambda - \mu| = C \tag{8}$$

where C is independent of λ. Actually, (8) has to hold only for λ for which $\sigma(\lambda) > 0$; one cannot add a negative increment to $\sigma(\lambda)$ where $\sigma(\lambda) = 0$ and (8) can not be derived for such λ. It is not difficult to solve (8). This will not be done, however, but the solution given and then verified.

Differentiation of (8) with respect to λ eliminates C. Before carrying it out, one must replace the integral by

$$\lim_{\epsilon \to 0} \left(\int_{-\infty}^{\lambda - \epsilon} d\mu + \int_{\lambda + \epsilon}^{\infty} d\mu \right) \sigma(\mu) \ln|\lambda - \mu|.$$

When this is differentiated with respect to λ, the terms arising from the differentiation of the limits drop out and only the derivative of $\ln|\lambda - \mu|$ remains. The integral becomes a principal value integral, or the arithmetic mean of two integrals in the complex plane, one contour C_+ above, the other contour C_- below the singularity at $\mu = \lambda$. Hence, (8) becomes

$$\int_{C+} \frac{d\mu\, \sigma(\mu)}{\lambda - \mu} + \int_{C-} \frac{d\mu\, \sigma(\mu)}{\lambda - \mu} = \lambda. \tag{8a}$$

Conversely, if (8a) is satisfied by some σ, (8) also will follow if σ is an even function. We try

$$\begin{aligned} \sigma(\mu) &= c(A^2 - \mu^2)^{\frac{1}{2}} && |\mu| < A \\ &= 0 && |\mu| > A. \end{aligned} \tag{9}$$

The sum of the two integrals on the left of (8a) can now be united to an integral going around all three singularities, at $\mu = -A, \lambda, A$.

Large Deviations of the Maximum Eigenvalue for Wishart and Gaussian Random Matrices

Satya N. Majumdar[1] and Massimo Vergassola[2]

[1]*Laboratoire de Physique Théorique et Modèles Statistiques (UMR 8626 du CNRS), Université Paris-Sud, Bâtiment 100, 91405 Orsay Cedex, France*

[2]*Institut Pasteur, CNRS URA 2171, F-75724 Paris 15, France*

(Received 14 November 2008; published 12 February 2009)

We present a Coulomb gas method to calculate analytically the probability of rare events where the maximum eigenvalue of a random matrix is much larger than its typical value. The large deviation function that characterizes this probability is computed explicitly for Wishart and Gaussian ensembles. The method is general and applies to other related problems, e.g., the joint large deviation function for large fluctuations of top eigenvalues. Our results are relevant to widely employed data compression techniques, namely, the principal components analysis. Analytical predictions are verified by extensive numerical simulations.

DOI: 10.1103/PhysRevLett.102.060601 PACS numbers: 05.40.−a, 02.10.Yn, 02.50.Sk, 24.60.−k

Rare events where one of the eigenvalues of a random matrix is much larger than the others play an important role in data compression techniques such as the ''Principal Components Analysis'' (PCA). PCA is helpful to detect hidden patterns or correlations in complex, high-dimensional datasets. A nonexhaustive list of applications includes image processing [1,2], biological microarrays [3,4], population genetics [5–7], finance [8,9], meteorology, and oceanography [10]. The main idea behind PCA is very simple. Consider a rectangular $(M \times N)$ matrix X whose entries represent some data. For instance, X_{ij} might represent examination marks of the i-th student ($1 \leq i \leq M$) in the j-th subject (physics, etc., with $1 \leq j \leq N$). The product symmetric matrix $W = X^\dagger X$ represents the covariance matrix of the data, and it contains information about correlations. In PCA, one first identifies eigenvalues and eigenvectors of W. The data are maximally scattered and correlated along the eigenvector (''principal component'') associated with the largest eigenvalue $\lambda_{\max}$. The scatter progressively reduces as lower and lower eigenvalues are considered. The subsequent step is the reduction of data dimensionality, achieved by setting to zero those components corresponding to low eigenvalues. The *rationale* is that retaining the largest components will preserve the major patterns in the data and only minor variations are filtered out.

The above description of PCA makes clear that its efficiency depends upon the gap between the top eigenvalues and the ''sea'' of smaller eigenvalues. In particular, the further is the maximum eigenvalue $\lambda_{\max}$ spaced from all the others, the more effective the projection and the compression procedure will be. A question naturally arises: how good is PCA for random data? This issue has a twofold interest. First, the data often are high-dimensional and have random components. Second, random ensembles provide null models needed to gauge the statistical significance of results obtained for nonrandom datasets. To address the question just formulated, one needs to compute the probability of rare events where the largest eigenvalue $\lambda_{\max}$ has atypically large fluctuations. The purpose of this Letter is to provide a simple physical method, based on the Coloumb gas method in statistical physics, that allows us to compute analytically the probability of these rare events for a general class of random matrices.

Let us start by considering Wishart matrices [11], which are directly related to PCA and multivariate statistics [12]. Wishart matrices are defined via the product $W = X^\dagger X$ of a $(M \times N)$ random matrix X having its elements drawn independently from a Gaussian distribution, $P[X] \propto \exp[-\frac{\beta}{2}\,\mathrm{Tr}(X^\dagger X)]$. The Dyson indices $\beta = 1$, 2 correspond, respectively, to real and complex X [13]. Without any loss of generality, we will assume hereafter that $M \geq N$. In addition to the aforementioned PCA applications, Wishart matrices appear in antenna selection in communi-

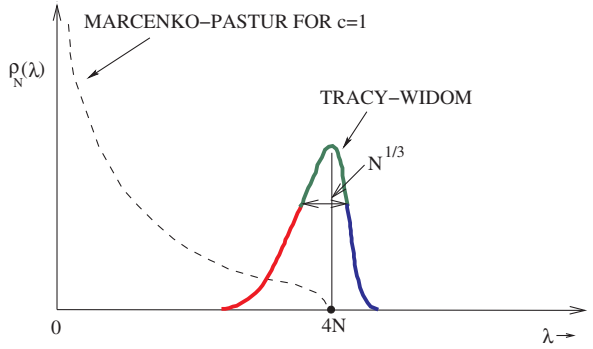

FIG. 1 (color online). The dashed line shows schematically the Marcenko-Pastur average density of states for Wishart matrices with the aspect-ratio parameter $c \equiv N/M = 1$; the full line is the distribution of the maximum eigenvalue $\lambda_{\max}$. The PDF is centered around the mean $\langle \lambda_{\max} \rangle = 4N$ and *typically* fluctuates over a scale of width $N^{1/3}$. The probability of fluctuations on this scale is described by the known Tracy-Widom distribution. The line on the right (left) describes the right (left) large deviation tail of the PDF, which is the object of interest in this Letter.

cation technology [14], nuclear physics [15], quantum chromodynamics [16], of directed polymers in random media [17], and nonintersecting Brownian motions [18].

The spectral properties of $W = X^\dagger X$ are well known: N eigenvalues $\{\lambda_i\}$'s of W are nonnegative random variables with a joint probability density function (PDF) [19]

$$P[\{\lambda_i\}] \propto e^{-(\beta/2)\sum_{i=1}^N \lambda_i} \prod_{i=1}^N \lambda_i^{\alpha\beta/2} \prod_{j<k} |\lambda_j - \lambda_k|^\beta, \quad (1)$$

where $\alpha = (1 + M - N) - 2/\beta$. This can be written as $P[\{\lambda_i\}] \propto \exp[-\beta E(\{\lambda_i\})/2]$, with the energy

$$E[\{\lambda_i\}] = \sum_{i=1}^N (\lambda_i - \alpha \log \lambda_i) - \sum_{j\neq k} \ln|\lambda_j - \lambda_k|, \quad (2)$$

coinciding with that of a 2-d Coulomb gas of charges with coordinates $\{\lambda_i\}$. Charges are confined to the positive half line in the presence of an external linear + logarithmic potential. The external potential tends to push the charges towards the origin, while the Coulomb repulsion tends to spread them apart. A glance at (2) indicates that these two competing mechanisms balance for values of λ scaling as $\sim N$. Indeed, from the joint PDF (1), one can calculate the average density of eigenvalues, $\rho_N(\lambda) = \frac{1}{N} \times \sum_{i=1}^N \langle \delta(\lambda - \lambda_i)\rangle \approx \frac{1}{N} f_{\rm MP}(\frac{\lambda}{N})$, with the Marcenko-Pastur (MP) [20] scaling function,

$$f_{\rm MP}(x) = \frac{1}{2\pi x}\sqrt{(b-x)(x-a)}. \quad (3)$$

Here, $c = N/M$ (with $c \leq 1$) and the upper and lower edges are $b = (c^{-1/2} + 1)^2$ and $a = (c^{-1/2} - 1)^2$. For all $c < 1$, the average density vanishes at both edges of the MP sea. For the special case $c = 1$, we have $a = 0$, $b = 4$ and the average density $f_{\rm MP}(x) = \frac{1}{2\pi}\sqrt{(4-x)/x}$ for $0 \leq x \leq 4$, diverges as $x^{-1/2}$ at the lower edge (see Fig. 1).

The MP expression shows that the maximum eigenvalue $\lambda_{\rm max}$ has the average value $\langle \lambda_{\rm max}\rangle \approx bN$ for large N. Typical fluctuations of $\lambda_{\rm max}$ are known to be of $O(N^{1/3})$ [12,17]. More specifically, $\lambda_{\rm max} = bN + c^{1/6} b^{2/3} N^{1/3} \chi$, where χ has an N-independent limiting PDF, $g_\beta(\chi)$, the well-known Tracy-Widom (TW) density [21]. The TW distribution for $\beta = 1, 2$ has asymmetric tails [21]

$$g_\beta(\chi) \sim \exp\left[-\frac{\beta}{24}|\chi|^3\right] \quad \text{as } \chi \to -\infty, \quad (4)$$

$$\sim \exp\left[-\frac{2\beta}{3}\chi^{3/2}\right] \quad \text{as } \chi \to \infty. \quad (5)$$

In contrast, *atypically large*, e.g., $\sim O(N)$, fluctuations of $\lambda_{\rm max}$ from its mean bN are not described by the TW distribution. Note that these fluctuations are precisely those that are relevant here for the PCA to work accurately.

What does the PDF $P(\lambda_{\rm max}, N)$ look like for $|\lambda_{\rm max} - bN| \gg O(N^{1/3})$ where the TW form is no longer valid? Using general large deviation principles, Johansson [17] proved that for large fluctuations $\sim O(N)$ from its mean, the PDF $P(\lambda_{\rm max} = t, N)$ has the form (for large N)

$$P(t,N) \sim \exp\left[-\beta N^2 \Phi_-\left(\frac{bN - t}{N}\right)\right] \; t \ll bN;$$
$$\sim \exp\left[-\beta N \Phi_+\left(\frac{t - bN}{N}\right)\right] \; t \gg bN; \quad (6)$$

where $\Phi_\pm(x)$ are the right (left) rate functions for the large positive (negative) fluctuations of $\lambda_{\rm max}$. The challenge is to explicitly compute their functional forms. The approach developed for Gaussian matrices [22] allows us to compute the left function $\Phi_-(x)$ [23] but it does not apply to the right tail. The problem of computing the right function $\Phi_+(x)$ is solved hereafter, followed by the application to Gaussian matrices and further generalizations.

The starting point of our method to compute $\Phi_+(x)$ is the energy expression (2). The MP distribution is obtained by the saddle-point method and holds even if all eigenvalues are constrained to be smaller than a threshold, provided the latter is larger than the upper edge b of the MP sea (see, e.g., [23]). This result and the Coulomb gas physics suggest that when the rightmost charge is moved to the right, $\lambda_{\rm max} - bN \sim O(N)$, the MP sea should *a priori* not be dragged and macroscopically rearranged. Following this physical picture, the right rate function is determined by the energy cost in pulling the rightmost charge in the external potential of the Coulomb gas and its interaction with the *unperturbed* MP sea. This energy cost for $\lambda_{\rm max} = t \gg bN$ can be estimated using Eq. (2)

$$\Delta E(t) = t - \alpha \ln(t) - 2N \int \ln|t - \lambda| \rho_N(\lambda) d\lambda, \quad (7)$$

where $\rho_N(\lambda)$ is the MP average density of charges and the integral describes the Coulomb interaction of the rightmost charge with the MP sea. This energy expression is valid up to an additive constant, chosen such that $\Delta E(t = bN) = 0$ since our reference configuration is the one where $\lambda_{\rm max} = bN$. For large N, we scale $t = zN$, use the MP expression (3) and the energy cost finally takes the form

$$\frac{\Delta E(z)}{N} = z - \frac{1-c}{c}\ln(z) - 2\int_a^b \ln(z - z') f_{\rm MP}(z') dz', \quad (8)$$

valid for $z \geq b$ and up to an additive constant. The probability of such a configuration is $P(z, N) \propto \exp[-\beta \Delta E(z)/2]$. Making a shift of variable $z = b + x$, it follows that $P(t, N)$ for large N and for $t - bN \sim O(N)$ agrees with the large deviation behavior in Eq. (6). Progress is that we also have derived the explicit expression of the right rate function $\Phi_+(x)$

$$\Phi_+(x) = \frac{x}{2} - \frac{1-c}{2c}\ln\left(\frac{x+b}{b}\right) - \int_a^b \ln\left(\frac{x + b - x'}{b - x'}\right) f_{\rm MP}(x') dx', \quad (9)$$

where $x > 0$ and the additive constant was chosen to have $\Phi_+(0) = 0$. The integral can be computed exactly as a hypergeometric function. For $c = 1$ ($a = 0$ and $b = 4$),

$$\Phi_+(x) = \frac{x+2}{2} - \ln(x+4) + \frac{1}{x+4} G\left(\frac{4}{4+x}\right), \quad (10)$$

where $G(z) = {}_3F_2[\{1, 1, 3/2\}, \{2, 3\}, z]$ is a hypergeometric function (with a lengthy but explicit expression in terms of elementary functions). For the sake of comparison, we also report the simpler expression of the left rate function [23]: $\Phi_-(x) = \ln(2/\sqrt{4-x}) - x/8 - x^2/64$ for $x \geq 0$.

The asymptotics of $\Phi_+(x)$ can be easily worked out from Eq. (9). For large x, $\Phi_+(x) \sim x/2$ independently of c, while the function has a nonanalytic behavior for small x:

$$\Phi_+(x) \approx \frac{\sqrt{b-a}}{3b} x^{3/2} \quad \text{as } x \to 0. \quad (11)$$

This shows that, as $\lambda_{\max} - bN \ll O(N)$ from the right side, the PDF of $\lambda_{\max} = t$ in Eq. (6) behaves as $\exp[-\beta N(\sqrt{b-a}/3b)(t/N - b)^{3/2}]$. Expressing the exponent in terms of the TW variable $\chi = c^{-1/6} b^{-2/3} N^{-1/3}(t - bN)$, we recover exactly the right tail behavior of the TW density in Eq. (5). Thus, the large deviation function $\Phi_+(x)$ matches, for small arguments x, the behavior of the TW density at large arguments. This is quite consistent with the fact that the scales of the fluctuations for TW and $\Phi_+(x)$ are $O(N^{1/3})$ and $O(N)$, respectively. In fact, our method provides, as a bonus, a physical derivation of the right tail behavior of the TW density [21].

We confirmed theoretical predictions by extensive numerical simulations. About 10^{11} realizations of real ($\beta = 1$) Wishart matrices of sizes $N = 10, 26, 50, 100$, and with different values of $c \leq 1$ were efficiently generated using the tridiagonal results in [24]. We find very good agreement with our analytical predictions for the right large deviations. For example, in Fig. 2, we present the results for $c = 1$ and $N = 10$. Monte Carlo numerical results are compared to the TW density (obtained by numerically integrating the Painlevé equation satisfied by the TW distribution [21]) and $\Phi_+(x)$ in Eq. (10), multiplied by N. For comparison, we also show the corresponding left rate function $\Phi_-(-x)$ [23] multiplied by N^2. It is clear that, while the numerical data are well described by the TW density near the peak of the distribution, they deviate considerably from TW as one moves into the tails, where our large deviation predictions work perfectly.

Our Coulomb gas method is quite general, and it can be applied to other related problems. For example, we can compute the right large deviation function of $\lambda_{\max}$ for Gaussian random matrices. For the latter, the eigenvalues can be positive or negative with joint PDF [25],

$$P[\{\lambda_i\}] \propto e^{-(\beta/2)\sum_{i=1}^N \lambda_i^2} \prod_{j<k} |\lambda_j - \lambda_k|^\beta, \quad (12)$$

where the Dyson indices $\beta = 1, 2$, and 4 correspond to the orthogonal, unitary, and symplectic ensembles. The quadratic nature of the potential in (12), in contrast to the linear term appearing in (1), makes that the amplitude of a typical eigenvalue scales as $\sim\sqrt{N}$. The average density of states for large N has the scaling form, $\rho_N(\lambda) \approx \frac{1}{\sqrt{N}} f_{\rm sc}(\frac{\lambda}{\sqrt{N}})$, where the famous Wigner semicircular law $f_{\rm sc}(x) = \sqrt{2-x^2}/\pi$ has compact support over $[-\sqrt{2}, \sqrt{2}]$. Thus, $\langle \lambda_{\max} \rangle = \sqrt{2N}$ and typical fluctuations of $\lambda_{\max}$ around its mean are known [21] to be TW distributed over a scale of $\sim O(N^{-1/6})$. Specifically, $\lambda_{\max} = \sqrt{2N} + a_\beta N^{-1/6} \chi$, with $a_{1,2} = 1/\sqrt{2}$, $a_4 = 2^{-7/6}$, and χ is a random variable with the TW distribution $g_\beta(\chi)$. Again, the TW form describes the PDF $P(\lambda_{\max} = t, N)$ only in the vicinity of $t = \sqrt{2N}$ over a small scale of $\sim O(N^{-1/6})$.

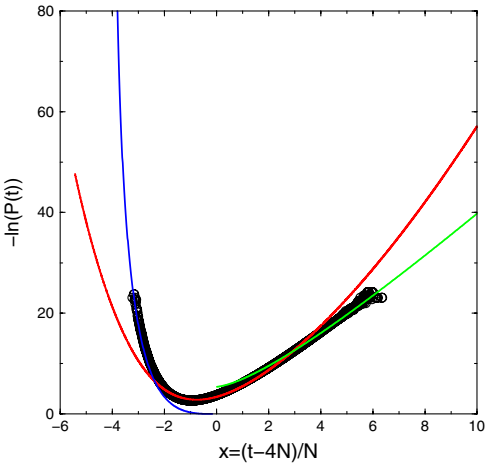

FIG. 2 (color online). Numerical results (circles) for the maximum eigenvalue distribution $-\ln P(\lambda_{\max} = t, N)$ vs the scaled variable $(t - 4N)/N$. Here, $N = 10$, Wishart matrices are real ($\beta = 1$) and $c = 1$. The Tracy-Widom distribution fits well the data for small fluctuations while it strongly deviates in both tails, where the agreement with large deviation predictions are excellent.

Fluctuations of $\lambda_{\max}$ over a scale $\sim O(\sqrt{N})$ are described by large deviation functions, analogous to the Wishart case in Eq. (6) but with a different scaling variable

$$P(t, N) \sim \exp\left[-\beta N^2 \Psi_-\left(\frac{\sqrt{2N} - t}{\sqrt{N}}\right)\right] \; t \ll \sqrt{2N};$$
$$\sim \exp\left[-\beta N \Psi_+\left(\frac{t - \sqrt{2N}}{\sqrt{N}}\right)\right] \; t \gg \sqrt{2N}.$$

As we mentioned, the left rate function $\Psi_-(x)$ was recently computed exactly in Ref. [22], but the right rate function $\Psi_+(x)$ was yet unknown. Our Coulomb gas approach allows us to solve this problem as well and gives for $\Psi_+(x)$

$$\Psi_+(x) = \frac{z^2 - 1}{2} - \ln(z\sqrt{2}) + \frac{1}{4z^2} G\left(\frac{2}{z^2}\right). \quad (13)$$

Here, $z = \lambda_{\max}/\sqrt{N} = x + \sqrt{2}$, the hypergeometric function G was defined earlier, and the additive constant was chosen to have $\Psi_+(0) = 0$. The asymptotics of $\Psi_+(x)$ can be easily derived: for large x, $\Psi_+(x) \sim x^2/2$, while the nonanalytic behavior $\Psi_+(x) \approx 2^{7/4} x^{3/2}/3$ holds for small x. Using the TW scaling variable $\chi = (\lambda_{\max} - \sqrt{2N}) N^{1/6}/a_\beta$, with a_β defined after (12), one recovers

the correct TW right tails for all $\beta = 1$, 2, and 4. This provides again a physical derivation of the TW right tail.

We have realized simulations for Gaussian matrices with sizes $N = 10$, 25, and 50 and for $\beta = 1$ and 2. In Fig. 3, we present the data for the PDF of $\lambda_{\max}$ (with $N = 10$, $\beta = 1$) and compare with the TW form and the exact left function Ψ_- [22] and right rate function $\Psi_+(x)$ derived in Eq. (13). As in the Wishart case, the TW form works well near the peak $t = \sqrt{2N}$, but it fails as we move into the tails, where the large deviation predictions are quite accurate.

Our Coulomb gas method lends to further generalizations that we only briefly mention here. For instance, we can compute the joint probability distribution for large fluctuations of n top eigenvalues in Wishart and Gaussian random matrices. If $n \ll N$, the energy will be given by their mutual charge interactions, the external potentials, and their interaction with the unperturbed MP sea. Integrals are the same as those computed previously and yield the explicit expression for the joint PDF. It is also possible to use our method to compute the large deviation function for fluctuations of the smallest eigenvalue $\lambda_{\min}$ for Wishart matrices with $c < 1$. Note that the MP sea remains unperturbed (and our method applies) for *small* fluctuations of $\lambda_{\min}$ while the method in [22] applies for large fluctuations of $\lambda_{\min}$, which compress the MP sea.

In conclusion, we have presented a new Coulomb gas method to compute large deviation probabilities of top eigenvalues for a general class of random matrices. The physical picture that emerges is quite transparent: when the top eigenvalues are pulled to the right (towards large values), the Marcenko-Pastur (or Wigner) sea is simply pinched and the top eigenvalues do not drag all the other eigenvalues. In other words, no macroscopic rearrangement of the sea occurs and the top eigenvalues move in the effective potential defined by the external potential of the Coulomb gas and by the electrostatic potential generated by the charges in the sea. Our predictions are formally valid for large N, yet our simulations indicate that they work for moderate N as well. This further adds to the relevance of the large deviation rate functions derived here to data compression methods and their applications.

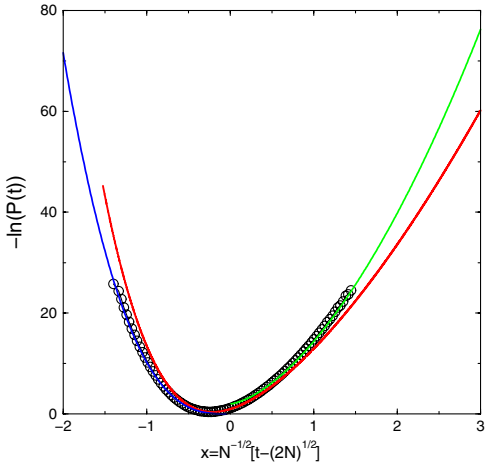

FIG. 3 (color online). Numerical results for the maximum eigenvalue distribution (circles) for $N = 10$ real ($\beta = 1$) Gaussian matrices. The Tracy-Widom distribution fits well the data for small fluctuations but deviates strongly in both tails, where the large deviation predictions are excellent.

We are grateful to E. Aurell for the invitations to KTH, where this work was initiated.

Note added in proof.—While the Letter was at the proof stage, we became aware that our result in Eq. (13), for the special case of GOE ($\beta = 1$), was derived by a different method in [26].

[1] S. S. Wilks, *Mathematical Statistics* (J. Wiley & Sons, New York, 1962).
[2] K. Fukunaga, *Introduction to Statistical Pattern Recognition* (Elsevier, New York, 1990).
[3] N. Holter *et al.*, Proc. Natl. Acad. Sci. U.S.A. **97**, 8409 (2000).
[4] O. Alter *et al.*, Proc. Natl. Acad. Sci. U.S.A. **97**, 10101 (2000).
[5] L.-L. Cavalli-Sforza, P. Menozzi, and A. Piazza, *The History and Geography of Human Genes* (Princeton Univ. Press, Princeton, NJ, 1994).
[6] N. Patterson, A. L. Price, and D. Reich, PLoS Genetics **2**, e190 (2006).
[7] J. Novembre and M. Stephens, Nat. Genet. **40**, 646 (2008).
[8] J.-P. Bouchaud and M. Potters, *Theory of Financial Risks* (Cambridge University Press, Cambridge, 2001).
[9] Z. Burda and J. Jurkiewicz, Physica A (Amsterdam) **344**, 67 (2004).
[10] R. W. Preisendorfer, *Principal Component Analysis in Meteorology and Oceanography* (Elsevier, New York, 1988).
[11] J. Wishart, Biom. J. **20**, 32 (1928).
[12] I. M. Johnstone, Ann. Stat. **29**, 295 (2001).
[13] F. J. Dyson, J. Math. Phys. (N.Y.) **3**, 140 (1962).
[14] M. Sadek, A. Tarighat, and A. H. Sayed, IEEE Trans. Signal Process. **55**, 1498 (2007).
[15] Y. V. Fyodorov and H.-J. Sommers, J. Math. Phys. (N.Y.) **38**, 1918 (1997); Y. V. Fyodorov and B. A. Khoruzhenko, Phys. Rev. Lett. **83**, 65 (1999).
[16] J. J. M. Verbaarschot, Phys. Rev. Lett. **72**, 2531 (1994).
[17] K. Johansson, Commun. Math. Phys. **209**, 437 (2000).
[18] G. Schehr *et al.*, Phys. Rev. Lett. **101**, 150601 (2008).
[19] A. T. James, Ann. Math. Stat. **35**, 475 (1964).
[20] V. A. Marcenko and L. A. Pastur, Math. USSR-Sb **1**, 457 (1967).
[21] C. Tracy and H. Widom, Commun. Math. Phys. **159**, 151 (1994); **177**, 727 (1996).
[22] D. S. Dean and S. N. Majumdar, Phys. Rev. Lett. **97**, 160201 (2006); Phys. Rev. E **77**, 041108 (2008).
[23] P. Vivo, S. N. Majumdar, and O. Bohigas, J. Phys. A **40**, 4317 (2007).
[24] I. Dumitriu and A. Edelman, J. Math. Phys. (N.Y.) **43**, 5830 (2002).
[25] E. P. Wigner, Proc. Cambridge Philos. Soc. **47**, 790 (1951).
[26] G. Ben-Arous *et al.*, Probab. Theory Relat. Fields **120**, 1 (2001).

Journal of Statistical Mechanics: Theory and Experiment
An IOP and SISSA journal

Top eigenvalue of a random matrix: large deviations and third order phase transition

Satya N Majumdar and Grégory Schehr

Université Paris-Sud, LPTMS, CNRS (UMR 8626), F-91405 Orsay Cedex, France
E-mail: satya.majumdar@u-psud.fr and Gregory.Schehr@u-psud.fr

Received 24 October 2013
Accepted for publication 4 December 2013
Published 31 January 2014

Online at stacks.iop.org/JSTAT/2014/P01012
doi:10.1088/1742-5468/2014/01/P01012

Abstract. We study the fluctuations of the largest eigenvalue $\lambda_{\max}$ of $N \times N$ random matrices in the limit of large N. The main focus is on Gaussian β ensembles, including in particular the Gaussian orthogonal ($\beta = 1$), unitary ($\beta = 2$) and symplectic ($\beta = 4$) ensembles. The probability density function (PDF) of $\lambda_{\max}$ consists, for large N, of a central part described by Tracy–Widom distributions flanked, on both sides, by two large deviation tails. While the central part characterizes the typical fluctuations of $\lambda_{\max}$—of order $\mathcal{O}(N^{-2/3})$—the large deviation tails are instead associated with extremely rare fluctuations—of order $\mathcal{O}(1)$. Here we review some recent developments in the theory of these extremely rare events using a Coulomb gas approach. We discuss in particular the third order phase transition which separates the left tail from the right tail, a transition akin to the so-called Gross–Witten–Wadia phase transition found in 2-d lattice quantum chromodynamics. We also discuss the occurrence of similar third order transitions in various physical problems, including non-intersecting Brownian motions, conductance fluctuations in mesoscopic physics and entanglement in a bipartite system.

Keywords: matrix models, random matrix theory and extensions, extreme value statistics

ArXiv ePrint: 1311.0580v2

1742-5468/14/P01012+31$33.00

Universal Fluctuations of Growing Interfaces: Evidence in Turbulent Liquid Crystals

Kazumasa A. Takeuchi* and Masaki Sano

Department of Physics, The University of Tokyo, 7-3-1 Hongo, Bunkyo-ku, Tokyo 113-0033, Japan

(Received 28 January 2010; published 11 June 2010)

We investigate growing interfaces of topological-defect turbulence in the electroconvection of nematic liquid crystals. The interfaces exhibit self-affine roughening characterized by both spatial and temporal scaling laws of the Kardar-Parisi-Zhang theory in $1 + 1$ dimensions. Moreover, we reveal that the distribution and the two-point correlation of the interface fluctuations are universal ones governed by the largest eigenvalue of random matrices. This provides quantitative experimental evidence of the universality prescribing detailed information of scale-invariant fluctuations.

DOI: 10.1103/PhysRevLett.104.230601 PACS numbers: 05.40.−a, 47.27.Sd, 64.70.mj, 89.75.Da

Growth phenomena have been a subject of extensive studies in physics and beyond, because of their ubiquity in nature and their importance in both engineering and fundamental science. Over recent decades, physicists have found that growth phenomena due to local processes typically lead to the formation of rough self-affine interfaces, as exemplified in paper wetting, burning fronts, bacterial colonies, and material morphology, to name but a few, and also in various numerical models [1]. Being obviously irreversible, local growth processes provide a challenging situation toward understanding the scale invariance and the consequent universality out of equilibrium.

The roughness of interfaces is often quantified by their width $w(l, t)$ defined as the standard deviation of the interface height $h(x, t)$ over a length scale l at time t. The self-affinity of interfaces then implies the following Family-Vicsek scaling [2]:

$$w(l, t) \sim t^{\beta} F(lt^{-1/z}) \sim \begin{cases} l^{\alpha} & \text{for } l \ll l_* \\ t^{\beta} & \text{for } l \gg l_*, \end{cases} \tag{1}$$

with two characteristic exponents α and β, the dynamic exponent $z \equiv \alpha/\beta$, and a crossover length scale $l_* \sim t^{1/z}$.

The simplest theory to describe such local growth processes was proposed by Kardar, Parisi, and Zhang (KPZ) [3] on the basis of the coarse-grained stochastic equation

$$\frac{\partial}{\partial t} h(x, t) = v_0 + \nu \nabla^2 h + \frac{\lambda}{2} (\nabla h)^2 + \xi(x, t) \tag{3}$$

with $\langle \xi(x, t) \rangle = 0$ and $\langle \xi(x, t) \xi(x', t') \rangle = D \delta(x - x') \delta(t - t')$. For $1 + 1$ dimensions, the renormalization group approach provides exact values of the exponents at $\alpha^{\mathrm{KPZ}} = 1/2$ and $\beta^{\mathrm{KPZ}} = 1/3$ [1,3], which are universal as widely confirmed in numerical models [1]. Moreover, the $(1 + 1)$-dimensional KPZ class attracts growing interest thanks to rigorous work on the asymptotic form of the fluctuations in solvable models [4–6]. This opens up a new aspect in the study of scale-invariant phenomena toward the universality beyond the scaling laws.

In contrast with such remarkable progress in theory, the situation in experiments has been quite different. A considerable number of experiments have been performed on various growth processes [1] and confirmed the ubiquity of rough interfaces. Concerning the universality, however, experimentally measured values of the exponents are widely diverse and mostly far from the KPZ values for both α and β [1]. To our knowledge, only two experiments among dozens directly found the KPZ exponents: in colonies of mutant bacteria [7] and in slow combustion of paper [8]; a few other experiments showed indirect indications [9,10]. One of the main difficulties shared by most experiments, including the above two, is that one needs to repeat a large number of experiments in the same controlled conditions to accumulate sufficient statistics. In this Letter, studying growing interfaces of turbulent liquid crystals, we overcome this difficulty and report clear experimental evidence of not only the universal scaling laws but also the universal fluctuations of the KPZ class through critical comparisons with the wealth of theoretical predictions.

The electroconvection occurs when an external voltage is applied to a thin layer of nematic liquid crystal, triggering the Carr-Helfrich instability [11]. We focus on interfaces between two topologically different turbulent states called the dynamic scattering modes 1 and 2 (DSM1 and DSM2), which are observed with sufficiently large voltages. The essential difference between them lies in the density of topological defects called the disclinations. Upon applying a voltage, we first observe the DSM1 state with practically no defects in the director field, which lasts until a disclination is finally created owing to the breakdown of surface anchoring [12]. This forms a DSM2 cluster composed of a large quantity of disclinations, which are constantly elongated, split, and transported by fluctuating turbulent flow around. While DSM2 may coexist with DSM1 in a regime of spatiotemporal intermittency [13], for larger voltages we observe growing DSM2 clusters driven by the above-mentioned stochastic local contamination processes.

Our experimental setup consists of a quasi-two-dimensional sample cell, an optical microscope, a thermocontroller, and an ultraviolet pulse laser (see Ref. [13] for

detailed descriptions). The cell is made of two parallel glass plates with transparent electrodes, which are spaced by a polyester film of thickness 12 μm enclosing a region of 16 mm $\times$ 16 mm for the convection. We chose here the homeotropic alignment of liquid crystals in order to work with isotropic DSM2 growth, which is realized by coating *N*, *N*-dimethyl-*N*-octadecyl-3-aminopropyltrimethoxysilyl chloride uniformly on the electrodes using a spin coater. The cell is then filled with *N*-(4-methoxybenzylidene)-4-butylaniline doped with 0.01 wt. % of tetra-*n*-butylammonium bromide. The cutoff frequency of the conductive regime [11] is 850 $\pm$ 50 Hz. The cell is maintained at a constant temperature 25.0 °C with typical fluctuations in the order of 10^{-3} K. The convection is observed through the transmitted light from light-emitting diodes and recorded by a CCD camera.

For each run we apply a voltage of 26 V at 250 Hz, which is sufficiently larger than the DSM1-DSM2 threshold at 20.7 V. After waiting a few seconds, we shoot into the cell two successive laser pulses of wavelength 355 nm and energy 6 nJ to trigger a DSM2 nucleus [13]. Figure 1 displays typical growth of a DSM2 cluster. We repeat it 563 times to characterize the growth process precisely.

We define the local radius $R(x, t)$ along the circle which denotes the statistically averaged shape of the droplets, as sketched in Fig. 1(b). This measures the interfacial width $w(l, t) \equiv \langle\sqrt{\langle[R(x, t) - \langle R\rangle_l]^2\rangle_l}\rangle$ and the height-difference correlation function $C(l, t) \equiv \langle[R(x + l, t) - R(x, t)]^2\rangle$, where $\langle\cdots\rangle_l$ and $\langle\cdots\rangle$ denote the average over a segment of length l and all over the interface and ensembles, respectively. Both $w(l, t)$ and $C(l, t)^{1/2}$ are common quantities for characterizing the roughness, for which the Family-Vicsek scaling [Eq. (1)] is expected.

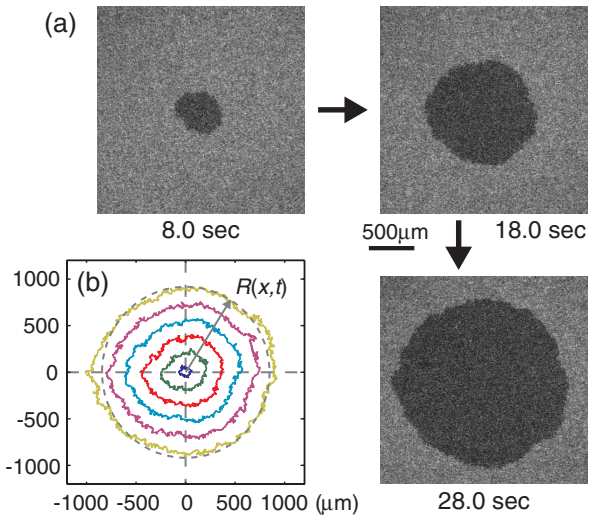

FIG. 1 (color online). Growing DSM2 cluster. (a) Images. Indicated below is the elapsed time after the emission of laser pulses. (b) Snapshots of the interfaces taken every 5 s in the range 2 s $\leq t \leq$ 27 s. The gray dashed circle shows the mean radius of all the droplets at $t = 27$ s. The coordinate x at this time is defined along this circle.

This is tested in Fig. 2. Raw data of $w(l, t)$ and $C(l, t)^{1/2}$ measured at different times [Figs. 2(a) and 2(b)] grow algebraically for short length scales $l \ll l_*$ and converge to constants for $l \gg l_*$ in agreement with Eq. (1). The power α of the algebraic regime measured in the last frame $t = 28.4$ s is found to be $\alpha = 0.50(5)$. Here, the number in the parentheses indicates the range of error in the last digit, which is estimated both from the uncertainty in a single fit and from the dependence on the fitting range. The found value of α is in good agreement with the KPZ roughness exponent $\alpha^{\mathrm{KPZ}} = 1/2$.

The temporal growth of the roughness is measured by the overall width $W(t) \equiv \sqrt{\langle[R(x, t) - \langle R\rangle]^2\rangle}$ and the plateau level of the correlation function, $C_{\mathrm{pl}}(t)^{1/2}$, defined as the mean value of $C(l, t)^{1/2}$ in the plateau region of Fig. 2(b). Both quantities show a very clear power law t^{β} with $\beta = 0.336(11)$ [Fig. 2(c)] in remarkable agreement with the KPZ growth exponent $\beta^{\mathrm{KPZ}} = 1/3$. Furthermore, rescaling both axes in Fig. 2(a) with the KPZ exponents, we confirm that our data of $w(l, t)$ collapse reasonably well onto a single curve [Fig. 2(d)]. A collapse of the same quality is obtained for $C(l, t)^{1/2}$. We therefore safely conclude that the DSM2 interfacial growth belongs to the (1 + 1)-dimensional KPZ class. In passing, this rules out the logarithmic temporal scaling claimed by Escudero for the droplet geometry [14].

Our statistically clean data motivate us to test further predictions on the KPZ class beyond those for the scaling. In this respect one of the most challenging benchmarks may be the asymptotic distribution of height fluctuations, calculated exactly for solvable models [5,6]. A general

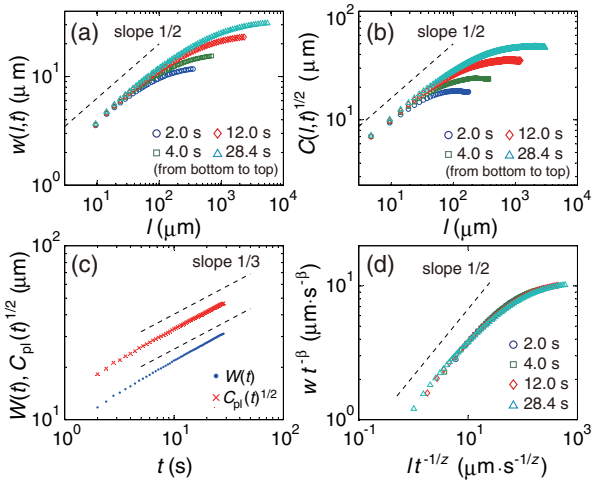

FIG. 2 (color online). Scaling of the width $w(l, t)$ and the height-difference correlation function $C(l, t)$. (a, b) Raw data of $w(l, t)$ (a) and $C(l, t)^{1/2}$ (b) at different times t. The length scale l is varied up to $2\pi\langle R\rangle$ and $\pi\langle R\rangle$, respectively. (c) Time evolution of the overall width $W(t)$ and the plateau level $C_{\mathrm{pl}}(t)^{1/2}$ of the correlation function. (d) Collapse of the data in (a) showing the Family-Vicsek scaling [Eq. (1)]. The dashed lines are guides for the eyes showing the KPZ scaling.

expression was proposed by Prähofer and Spohn [6], which reads $h(t) \simeq v_\infty t + (A^2\lambda t/2)^{1/3}\chi$ with $A \equiv D/2\nu$, the asymptotic growth rate v_∞, and a random variable χ obeying the Tracy-Widom (TW) distribution [15], or the (rescaled) largest eigenvalue distribution of large random matrices. The random matrices are from the Gaussian unitary and orthogonal ensemble (GUE and GOE) [16] for curved and flat interfaces, respectively. This implies an intriguing relation to the random matrix theory and requires no fitting parameter provided that the values of the two KPZ parameters λ and A are measured. The prediction was tested once for flat interfaces in the paper combustion experiment [17] with an apparent agreement. However, the authors had to shift and rescale the distribution function for want of the values of the KPZ parameters, in which case the difference among the predicted distributions and the Gaussian one is unpronounced. They also had to discard data subject to intermittent advance of burning fronts due to quenched disorder [17]. Therefore, a quantitative test of Prähofer and Spohn's prediction has not been carried out so far.

We first measure the value of λ experimentally. For the circular interfaces, λ is given as the asymptotic radial growth rate, which has a leading correction term as $\lambda \simeq d\langle R\rangle/dt + a_v t^{-2/3}$ for $t \to \infty$ [18]. This relation is indeed confirmed in Fig. 3(a) and yields a precise estimate at $\lambda = 35.40(23)\ \mu$m/s.

The parameter A can be determined, at least for flat interfaces, from the amplitude of $C(l, t)$ and $w(l, t)$ through $C \simeq Al$ and $w^2 \simeq Al/6$ in the limit $t \to \infty$ [18]. Figure 3(b) shows $C(l, t)/l$ against l for different times t. A similar series of plots is obtained for $6w^2/l$. The value of A can be estimated from the plateau level or the local maximum of these plots, but we find that these estimates increase slowly with time and do not agree with each other (inset). This allows us to have only a rough estimate $A \approx 10\ \mu$m for the range of time we study.

Now we test Prähofer and Spohn's prediction for the circular interfaces:

$$R(t) \simeq \lambda t + (A^2\lambda t/2)^{1/3}\chi_{\mathrm{GUE}} \qquad (4)$$

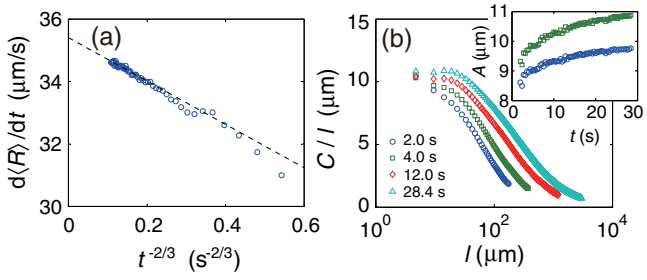

FIG. 3 (color online). Parameter estimation. (a) Growth rate $d\langle R\rangle/dt$ averaged over 1.0 s against $t^{-2/3}$. The y intercept of the linear regression (dashed line) provides an estimate of λ. (b) $C(l, t)/l$ against l for different times t. Inset: nominal estimates of A obtained from $w(l, t)$ (blue bottom symbols) and $C(l, t)$ (green top symbols) as functions of t (see text).

with a random variable χ_{GUE} obeying the GUE TW distribution. We first compute the cumulant $\langle R^n\rangle_c$, for which Eq. (3) implies $\langle R^n\rangle_c \simeq (A^2\lambda/2)^{n/3}\langle\chi^n_{\mathrm{GUE}}\rangle_c t^{n/3}$ for $n \geq 2$. Our data indeed show this power-law behavior in time [Fig. 4(a)], though higher order cumulants are statistically more demanding and hence provide less conclusive results. We then calculate the skewness $\langle R^3\rangle_c/\langle R^2\rangle_c^{3/2}$ and the kurtosis $\langle R^4\rangle_c/\langle R^2\rangle_c^2$, which do not depend on the parameter estimates. The result in Fig. 4(b) shows that both amplitude ratios asymptotically converge to the values of the GUE TW distribution, about 0.2241 for the skewness and 0.09345 for the kurtosis [6], and clearly rules out the GOE TW and Gaussian distributions. Conversely, if we admit the GUE TW distribution, the amplitude of $\langle R^2\rangle_c$ offers a precise estimate of A at 9.98(7) μm, which is consistent with the direct estimate obtained above and hence used in the following.

Histograms of the local radius $R(x, t)$ are then made and shown in Fig. 4(c) for two different times as functions of $q \equiv (R - \lambda t)/(A^2\lambda t/2)^{1/3}$, which corresponds to χ_{GUE} if Eq. (3) holds. The experimental distributions show remarkable agreement with the GUE TW one without any fitting, apart from a slight horizontal translation. Indeed, time series of the difference between the nth order cumulants of q and χ_{GUE} [Fig. 4(d)] reveal that the second to fourth order cumulants of q converge quickly to the GUE TW

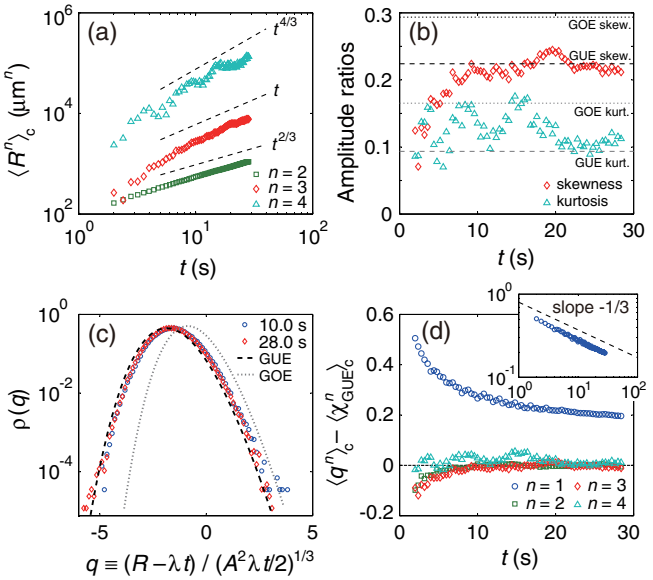

FIG. 4 (color online). Local radius distributions. (a) Cumulants $\langle R^n\rangle_c$ vs t. The dashed lines are guides for the eyes showing the indicated powers. (b) Skewness $\langle R^3\rangle_c/\langle R^2\rangle_c^{3/2}$ and kurtosis $\langle R^4\rangle_c/\langle R^2\rangle_c^2$. The dashed and dotted lines indicate the values of the skewness and the kurtosis of the GUE and GOE TW distributions. (c) Local radius distributions as functions of $q \equiv (R - \lambda t)/(A^2\lambda t/2)^{1/3}$. The dashed and dotted lines show the GUE and GOE TW distributions, respectively. (d) Differences in the cumulants of q and χ_{GUE}. The dashed line indicates $\langle q^n\rangle_c = \langle\chi^n_{\mathrm{GUE}}\rangle_c$. Inset: the same data for $n = 1$ in logarithmic scales. The dashed line is a guide for the eyes.

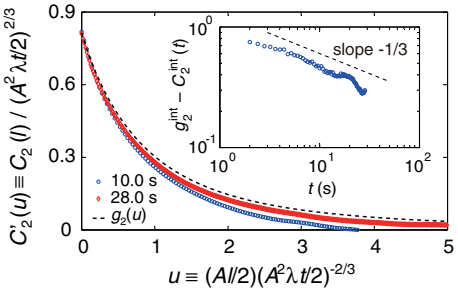

FIG. 5 (color online). Two-point correlation function $C_2(l, t)$ plotted in the rescaled axes $u \equiv (Al/2)(A^2\lambda t/2)^{-2/3}$ and $C_2'(u) \equiv C_2(l)/(A^2\lambda t/2)^{2/3}$. The dashed line indicates the theoretical prediction $g_2(u)$. Inset: integral of the rescaled correlation function $C_2^{\text{int}} \equiv \int_0^\infty C_2'(u)du$ as a function of time t. The difference from the theoretical counterpart $g_2^{\text{int}} \equiv \int_0^\infty g_2(u)du$ is shown. The dashed line is a guide for the eyes.

values, while the first order one, i.e., the mean, algebraically approaches it with a power close to $-1/3$ (inset). This is theoretically reasonable behavior which stems from the existence of an additional constant term in Eq. (3). Therefore, we conclude that the local radii of the DSM2 nuclei asymptotically obey the GUE TW distribution at least up to the fourth order cumulants, confirming the prediction of Prähofer and Spohn.

We also measure the two-point correlation function $C_2(l, t) \equiv \langle R(x + l, t)R(x, t)\rangle - \langle R\rangle^2$. Theory predicts that $C_2(l, t)$ is asymptotically described by the Airy$_2$ process $\mathcal{A}_2(t)$ or by the dynamics of the largest eigenvalue in Dyson's Brownian motion of GUE matrices [16] as $C_2(l, t) \simeq (A^2\lambda t/2)^{2/3} g_2(u)$ with $g_2(u) \equiv \langle \mathcal{A}_2(u + t)\mathcal{A}_2(t)\rangle$ and $u \equiv (Al/2)(A^2\lambda t/2)^{-2/3}$ [19]. Our experimental data confirm this with an algebraic finite-time correction consistent with the power $-1/3$ (Fig. 5).

In comparison with past experimental studies showing diverse scalings, one may wonder why the liquid crystal turbulence exhibits such clear KPZ-class behavior. We consider that the following three factors are essential. (i) The growth of DSM2 results from strictly local processes due to the turbulent flow on the interfaces and not from inward or outward interactions of the cluster, which could induce long-range effects and affect the universality. (ii) The stochasticity of the process stems from intrinsic turbulent fluctuations overwhelming quenched disorder. (iii) Good controllability and fast response of the liquid crystals allowed us to repeat hundreds of experiments in the same conditions, leading to statistically reliable data. The reproducibility of the presented results was confirmed with different voltages and spatial resolutions with the same quality of data (not shown).

In conclusion, measuring the growth of DSM2 nuclei in the electroconvection, we have found the circular interface roughening clearly characterized by the scaling laws of the KPZ class in 1 + 1 dimensions. Moreover, we have shown without fitting that the fluctuations of the cluster local radius asymptotically obey the Tracy-Widom distribution of the GUE random matrices and revealed the finite-time effect. Together with the agreement in the two-point correlation, our experimental results quantitatively confirm the geometry-dependent universality of the (1 + 1)-dimensional KPZ class prescribing detailed information of the scale-invariant fluctuations. In this respect, investigations of flat interfaces in the same system are of outstanding importance and are in progress.

We acknowledge enlightening discussions with H. Chaté, M. Prähofer, T. Sasamoto, and H. Spohn. We also thank M. Prähofer and F. Bornemann for providing us with numerical values of the TW distributions and the covariance of the Airy$_2$ process. This work is partly supported by JSPS and by MEXT (No. 18068005).

Note added in proof.—After submission of this Letter, Sasamoto and Spohn reported an exact solution of the (1 + 1)-dimensional KPZ equation [20], which offers a clear theoretical ground of our experimental results.

*kazumasa@daisy.phys.s.u-tokyo.ac.jp

[1] A.-L. Barabási and H. E. Stanley, *Fractal Concepts in Surface Growth* (Cambridge University Press, Cambridge, England, 1995).
[2] F. Family and T. Vicsek, J. Phys. A **18**, L75 (1985).
[3] M. Kardar, G. Parisi, and Y.-C. Zhang, Phys. Rev. Lett. **56**, 889 (1986).
[4] H. Spohn, Physica (Amsterdam) **369A**, 71 (2006).
[5] K. Johansson, Commun. Math. Phys. **209**, 437 (2000).
[6] M. Prähofer and H. Spohn, Physica A (Amsterdam) **279**, 342 (2000); Phys. Rev. Lett. **84**, 4882 (2000).
[7] J. Wakita *et al.*, J. Phys. Soc. Jpn. **66**, 67 (1997).
[8] J. Maunuksela *et al.*, Phys. Rev. Lett. **79**, 1515 (1997); M. Myllys *et al.*, Phys. Rev. E **64**, 036101 (2001).
[9] M. Degawa *et al.*, Phys. Rev. Lett. **97**, 080601 (2006).
[10] J. Kertész, V. K. Horváth, and F. Weber, Fractals **1**, 67 (1993); T. Engøy *et al.*, Phys. Rev. Lett. **73**, 834 (1994).
[11] P. G. de Gennes and J. Prost, *The Physics of Liquid Crystals* (Oxford Univ. Press, Oxford, 1993), 2nd ed.
[12] V. S. U. Fazio and L. Komitov, Europhys. Lett. **46**, 38 (1999).
[13] K. A. Takeuchi *et al.*, Phys. Rev. Lett. **99**, 234503 (2007); Phys. Rev. E **80**, 051116 (2009).
[14] C. Escudero, Phys. Rev. Lett. **100**, 116101 (2008); see also a Comment by J. Krug, *ibid.* **102**, 139601 (2009).
[15] C. A. Tracy and H. Widom, Commun. Math. Phys. **159**, 151 (1994); **163**, 33 (1994); **177**, 727 (1996).
[16] M. L. Mehta, *Random Matrices* (Elsevier, Amsterdam, 2004), 3rd ed..
[17] L. Miettinen *et al.*, Eur. Phys. J. B **46**, 55 (2005).
[18] J. Krug, P. Meakin, and T. Halpin-Healy, Phys. Rev. A **45**, 638 (1992); J. G. Amar and F. Family, *ibid.* **45**, 5378 (1992).
[19] M. Prähofer and H. Spohn, J. Stat. Phys. **108**, 1071 (2002); F. Bornemann, P. L. Ferrari, and M. Prähofer, *ibid.* **133**, 405 (2008).
[20] T. Sasamoto and H. Spohn, Phys. Rev. Lett. **104**, 230602 (2010).

PHYSICAL REVIEW E **85**, 020101(R) (2012)

Measuring maximal eigenvalue distribution of Wishart random matrices with coupled lasers

Moti Fridman, Rami Pugatch, Micha Nixon, Asher A. Friesem, and Nir Davidson*
Weizmann Institute of Science, Department of Physics of Complex Systems, Rehovot 76100, Israel
(Received 16 December 2011; published 1 February 2012)

We determined the probability distribution of the combined output power from 25 coupled fiber lasers and show that it agrees well with the Tracy-Widom and Majumdar-Vergassola distributions of the largest eigenvalue of Wishart random matrices with no fitting parameters. This was achieved with 500 000 measurements of the combined output power from the fiber lasers, that continuously changes with variations of the fiber lasers lengths. We show experimentally that for small deviations of the combined output power over its mean value the Tracy-Widom distribution is correct, while for large deviations the Majumdar-Vergassola distribution is correct.

DOI: 10.1103/PhysRevE.85.020101 PACS number(s): 05.40.−a, 02.10.Yn, 42.55.Wd, 42.60.Da

Random matrix theory has been exploited in numerous research fields ranging from nuclear spectra to quantum transport, models of quantum gravity in two dimensions, mesoscopic nonlinear dynamics, atomic physics, wireless communications, and multidimensional data analysis [1–5]. Of special interest are the minimal and maximal eigenvalues of random matrices, that determines for example the conductance fluctuations in two- and three- dimensional Anderson insulators [6,7]. An analytical expression describing typical deviations of the maximal eigenvalue was presented in the 1990s by Tracy and Widom (TW) [8,9] initiating many further theoretical developments in random matrix theory [10,11]. Recently, Majumdar and Vergassola (MV) calculated the probability of large deviations of the maximal eigenvalue [12–14] above the mean and Pierpaolo, Majumdar, and Bohigas (PMB) calculated below the mean. The MV and the PMB distributions were numerically confirmed, but so far eluded experimental demonstration.

In this Rapid Communication, we provide the first experimental observation of the MV and PMB distributions in a physical system and connect the field of coupled random lasers to random matrix theory. We report our measured distribution of the combined output power from an array of 25 coupled fiber lasers whose cavity lengths randomly fluctuate in time. We found that the measured distribution of the combined output power agrees well with the distribution of maximal eigenvalue of Wishart random matrices as predicted by TW and MV. For deviations close to the mean value, the measured distribution is shown to have a universal shape that agrees with the TW distribution. For large deviations from the mean value the measured distribution deviates from the TW distribution, but agrees well with the MV and PMB distributions over more than five decades with no fitting parameters. To account for this agreement, we present a heuristic model that illustrates the relation between the output power distribution from our array of coupled lasers to the maximal eigenvalue of Wishart random matrices.

Our experiment consisted of an array of 25 coupled fiber lasers schematically presented in Fig. 1. Each fiber laser was comprised of a ytterbium doped double clad fiber with lengths that varied from 1.3 m to 1.7 m, a high reflecting fiber Bragg grating (FBG) at the rear end of the fiber, and a low reflecting FBG at the front of the fiber. Each fiber lasers was end pumped by a stabilized diode laser of 975 nm wavelength. The length of each fiber laser was about 5 m and the output wavelength was 1070 nm with a bandwidth of 10 nm. Accordingly, there were 100 000 available frequencies (longitudinal modes) for each laser. The light emerging from all the fiber lasers was collected with a lens that was focused onto a detector to obtain the combined output power. The fiber lasers were arranged in 5×5 array, where the coupling between them was achieved by means of four coupling mirrors. By controlling the orientations of the coupling mirrors we could realize a variety of connectivities for the fiber lasers in the array, and in our experiments we concentrated on the one-dimensional and two-dimensional connectivities. Details about the experimental configuration, coupling arrangement, and connectivity manipulations were presented in previous work [15].

The lasers were operated close to threshold to maximize mode competition and ensure that lasing will only occur at the mode where the losses are minimal [16,17]. We measured the combined output power from the array over a duration of 60 hours. The correlation time of the output power fluctuations was found to be shorter than 0.5 s; hence we obtained over 500 000 uncorrelated measurements. Representative results of the combined output power over its mean as a function of time, with and without coupling between the lasers, are presented in Fig. 2. These are shown over a relatively short time duration, but their behavior was similar throughout the 60 hours measurement. As seen, the power fluctuations with coupling (dashed curve) are much larger than those without coupling between the lasers (solid curve), indicating that the fluctuations result from the coupling between the lasers [18].

Next we compared the measured results to the distribution of the largest eigenvalues of Wishart random matrices. Figure 3 presents the probability distributions of the measured output power in a one-dimensional connectivity (circles) and in a two-dimensional connectivity (asterisks) where the position of the maximum is chosen according to the maximum of the TW distribution (solid curve) [19]. We present the TW distribution using the scaled units [12]

$$x = \frac{t - 4N}{N}, \tag{1}$$

*nir.davidson@weizmann.ac.il

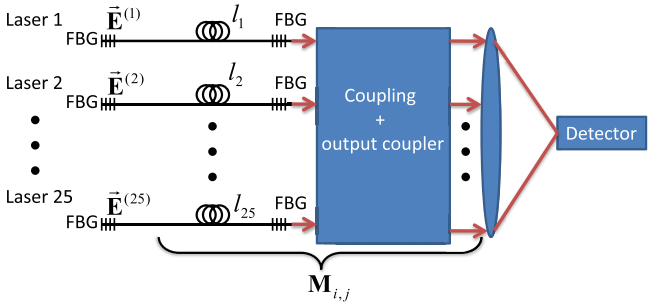

FIG. 1. (Color online) Experimental arrangement for measuring the combined output power distribution of 25 coupled fiber lasers. FBG, fiber Bragg gratings that serve as rear mirror (>99% reflectivity) and front mirrors (∼5% reflectivity); $E^{(i)}$, the complex electric field in the ith fiber near the rear FBG for each fiber laser; l_i, the length of the ith fiber. $M_{i,j}$ corresponds to the propagation matrix for a single round trip in the cavity and includes the propagation in each fiber, the output coupler (∼2% reflectivity), and the coupling between the different fibers (∼8% coupling). The light emerging from all the fiber lasers was collected with a lens that was focused onto a detector to obtain the combined output power. Details about the experimental configuration, coupling arrangement, and connectivity manipulations were presented in previous work [15].

where t is the largest eigenvalue and N is the matrix size. As evident, there is a very good agreement between the probability distributions of the experimental results and the TW distribution both for the one-dimensional connectivity and for the two-dimensional connectivity.

For closer inspection of the tails of the measured distributions, we present in Fig. 4 the probability distributions of the measured combined output power, for one-dimensional connectivity [circles, Fig. 4(a)] and two-dimensional connectivity [asterisks, Fig. 4(b)], together with the TW distribution (solid curves) and MV and PMB distributions (dashed curves) on a logarithmic scale. The insets illustrate the connectivities between the 25 fiber lasers [15].

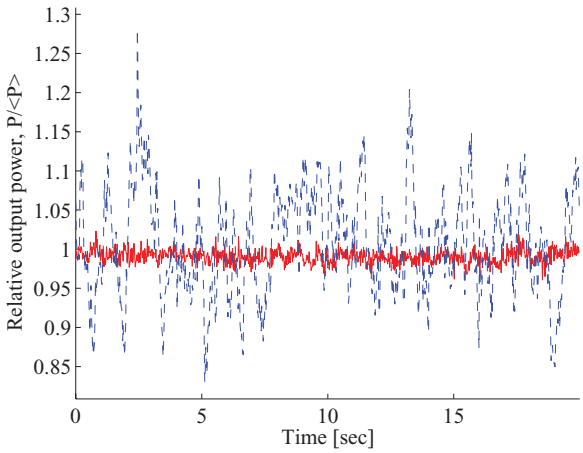

FIG. 2. (Color online) Representative experimental results of the combined output power from the 25 fiber lasers as a function of time. Solid curve (red) - without coupling between the lasers; Dashed curve (blue) - with coupling between the lasers. These results indicate that the fluctuations are caused by the coupling between the lasers.

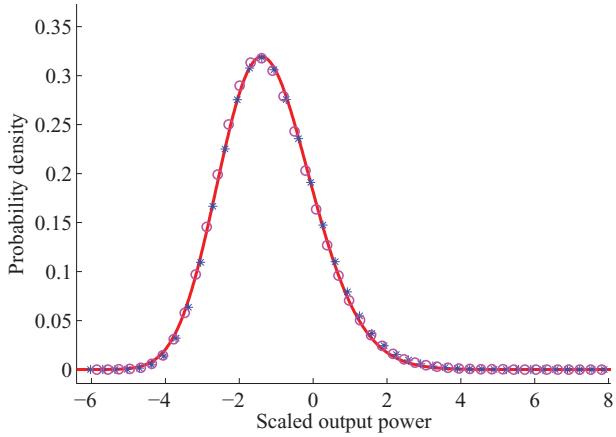

FIG. 3. (Color online) Probability distribution of the scaled combined output power. Circles, experimental results in a one-dimensional connectivity; asterisks, experimental results in a two-dimensional connectivity; solid curve, Tracy-Widom (TW) distribution. As seen, there is a very good agreement between the probability distributions of the experimentally measured results and the TW distribution in linear scale for both connectivities. For closer inspection of the fit to the tails of the distribution see Fig. 4.

The PMB distribution, plotted with no fitting parameters, is [14]

$$P(x) = c_1 \exp[-N^2 \Phi_-(-x)] \tag{2}$$

and the MV is [12]

$$P(x) = c_2 \exp\left[-N\ \Phi_+(x)\right], \tag{3}$$

where $c_1 = 0.5$ and $c_2 = 0.0063$ were found using numerical simulation in [12], and the functions $\Phi_+(x)$ and $\Phi_-(x)$ are

$$\Phi_+(x) = \frac{x}{2} + 1 - \ln(x+4) + \frac{1}{x+4} G\left(\frac{4}{4+x}\right) \tag{4}$$

and

$$\Phi_-(x) = \ln\left(\frac{2}{\sqrt{4-x}}\right) - \frac{x}{8} - \frac{x^2}{64}, \tag{5}$$

with $G(z) = {}_3F_2[\{1,1,3/2\},\{2,3\},z]$ a hypergeometric function.

As evident from Fig. 4, there are significant systematic deviations of the measured distribution from the TW distribution, both at values which are much larger or much smaller than the mean value [12–14]. However, there is a very good agreement between the experimental results and the MV and the PMB distributions for both connectivities, without any fitting parameters. The experimental results of the one-dimensional and the two-dimensional connectivities are essentially identical indicating the universality of the maximal eigenvalue distribution.

In order to illustrate the relation between the distribution of the measured power fluctuations and the maximal eigenvalues of Wishart random matrices, we developed a simple linear model. While an array of coupled fiber lasers is essentially a nonlinear system, many of its properties can be determined by its linearized round trip propagation matrix [16]. For example, the eigenvectors of this matrix correspond to the various global modes of the array while the eigenvalues are $\lambda_n = 1 - \alpha_n$,

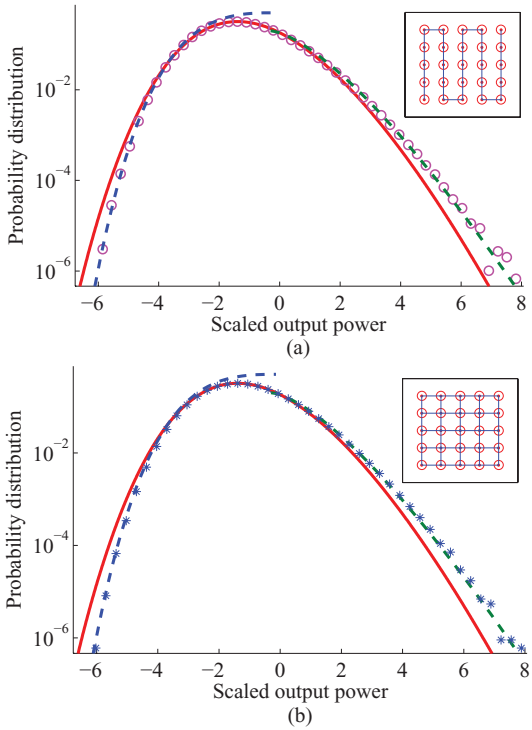

FIG. 4. (Color online) Probability distribution of the scaled combined output power for (a) one-dimensional connectivity (circles), and (b) two-dimensional connectivity (asterisks) in logarithmic scale. Solid curves, Tracy-Widom (TW) distribution; dashed curves, Majumdar-Vergassola (MV) distribution for eigenvalues much larger (right green) and Pierpaolo, Majumdar, and Bohigas (PMB) distribution for eigenvalues much smaller (left blue) than the mean, with no fitting parameters. As seen, at the tails of the measured distribution there are significant systematic deviations from the TW distribution. However, there is a very good agreement for both connectivities, between the measured results and the MV and PMB distributions at values which are much larger and much smaller from the mean value, respectively. Insets illustrate the connectivities between the 25 fiber lasers in each case [15].

where α_n is the loss of mode n [20,21]. The tendency of lasers to minimize losses will lead the coupled lasers to operate in the eigenmode corresponding to the largest eigenvalue [17,22].

We start by letting the electric field $E^{(i)}$ near the rear FBG of each fiber laser be a component of a vector of the total input field $|E_0\rangle$ (see Fig. 1). After propagating one round trip, the field $|E_1\rangle$ can be described as $|E_1\rangle = \mathbf{M}|E_0\rangle$, where $\mathbf{M}$ is a 25×25 round trip propagation matrix. Details on the derivation of a round trip propagation matrix are presented in [21]. Specifically, the elements along the diagonal of $\mathbf{M}$ denote the self-feedback light for each laser, as

$$\mathbf{M}_{i,i} = (1 - 4\kappa)e^{2ik_i l_i}, \tag{6}$$

where κ is the coupling strength between two adjacent lasers, l_i the length of the ith fiber laser, and k_i the wave vector of the ith laser out of all the 100 000 available frequencies. The off-diagonal elements of $\mathbf{M}$ denote the coupling between the lasers. For adjacent lasers which are not coupled the corresponding elements are zero. However, when the adjacent lasers are coupled the corresponding elements above the diagonal are

$$\mathbf{M}_{i,j} = \kappa e^{ik_i(l_i+l_j)}, \tag{7}$$

and below the diagonal the elements are

$$\mathbf{M}_{i,j} = \kappa e^{ik_j(l_i+l_j)}. \tag{8}$$

In a resonant cavity at steady state, the vector $|E_1\rangle$ should be one of the eigenvectors of $\mathbf{M}$, so $|E_1\rangle = \lambda_n |E_0\rangle$ where λ_n is inversely proportional to the losses in a single round trip. For many round trips, a complex λ_n will increase the losses due to interference. These considerations imply that to ensure minimal losses in the combined cavity λ_n should be real and maximal [16]. Due to the mode competition between the eigenvectors of $\mathbf{M}$ on the nonlinear gain, the coupled lasers will lase at the mode with the minimal losses [17], which corresponds to the eigenvector of the round trip propagation matrix with the maximal real eigenvalue. For high gain lasers such as fiber lasers, the output power of a mode is proportional to its eigenvalue [21]. Therefore, the combined output power of the array provides a direct measure for the value of the largest eigenvalue of the propagation matrix.

Due to thermal and acoustical fluctuations the length of each fiber laser changes rapidly such that $l_i k_i \mod 2\pi$ is effectively a random phase [18,23]. These random phases, after each variation in the fiber lengths, result in a different random round trip propagation matrix. The time scale of the length fluctuations in our system is much longer than the relaxation oscillation time of the lasers [16], justifying the steady state assumption. Accordingly, the distribution of the combined output power from the array fits the distribution of the largest eigenvalue of random matrices.

The probability for finding a single common wave vector k such that all the lasers in the array will have the same phase and a real valued λ_n is exponentially small in the number of lasers and is $\sim 10^{-5}$ for 25 lasers [24,25]. So, when the length of the fibers is set after each fluctuation, the lasers try to find the k vector which will satisfy the highest number of lasers. Therefore, the lasers group in several clusters, each with its own wave vector [26]. In each cluster the coupling can be either $+\kappa$ or $-\kappa$. Since the light that is coupled from one cluster to the other is essentially lost, the structure of the round trip propagation matrix M is block diagonal, where the elements along the diagonal are $1 - 4\kappa$ and the off-diagonal elements when there is coupling between two specific lasers are $\pm\kappa$. So after each fluctuation we have a different matrix where the blocks sizes and locations and the signs of the off-diagonal elements are random. To show that such a round trip propagation matrix $\mathbf{M}$ fall on the Wishart random matrix universality class, we simulated 10^4 different random realizations of our array with small (~ 10 μm) fluctuations in the lengths of each fiber. In each realization we found the clusters with common wave vector that yield minimal losses and obtained the corresponding round trip propagation matrix $\mathbf{M}$ [27]. Since $\mathbf{M}$ represents the round trip propagation in the cavity we can define a matrix $\mathbf{X}$ which represents a single pass in the cavity, so, $\mathbf{M} = \mathbf{X}\mathbf{X}^T$. We evaluated the probability distribution of each element in $\mathbf{X}$ and found it to have a Gaussian shape (data not shown), indicating that the round trip

propagation matrix **M** is indeed a Wishart matrix. Therefore, the distribution of the combined output power from the array should fit to the TW, MV and PMB distributions.

To conclude, we presented an experimental configuration of 25 coupled fiber lasers and showed that the probability distribution of their combined output power agrees well with the distribution of the largest eigenvalue of Wishart random matrices, namely the Tracy-Widom, Majumdar-Vergassola and Pierpaolo-Majumdar-Bohigas distributions. We believe that such a configuration can be extended to investigate symplectic and non-Hermitian random matrices with various connectivities by varying the polarizations and the losses in the fiber lasers. Moreover, while in this Rapid Communication we investigated the combined output power from an array of coupled lasers operating close to threshold, it is possible to operate the lasers far above their threshold and to investigate the phase locking across the array [15,27]. Such measurement of phase locking gives a direct measure for the number of lasers in each cluster and thereby enables investigation of coupled ensembles of oscillators where a common frequency for all the oscillators cannot be found.

This research was supported by the Israeli Ministry of Science and Technology and by the USA-Israel Binational Science Foundation. We are grateful to Eugene Kanzieper for his helpful comments.

[1] E. P. Wigner, Proc. Cambridge Philos. Soc. **47**, 790 (1951).
[2] C. W. J. Beenakker, Rev. Mod. Phys. **69**, 731 (1997).
[3] M. L. Mehta, *Random Matrices*, 2nd ed. (Academic Press, New York, 1991).
[4] F. Franchini and V. E. Kravtsov, Phys. Rev. Lett. **103**, 166401 (2009).
[5] P. Carpena, P. Bernaola-Galvan, M. Hackenberg, A. V. Coronado, and J. L. Oliver, Phys. Rev. E **79**, 035102(R) (2009).
[6] A. M. Somoza, M. Ortuno, and J. Prior, Phys. Rev. Lett. **99**, 116602 (2007).
[7] C. Monthus and T. Garel, Phys. Rev. B **80**, 024203 (2009).
[8] C. A. Tracy and H. Widom, Phys. Lett. B. **305**, 115 (1993).
[9] C. A. Tracy and H. Widom, Commun. Math. Phys. **159**, 151 (1994).
[10] K. Johansson, Commun. Math. Phys. **209**, 437 (2000).
[11] T. Tao and V. Vu, Ann. Stat. **38**, 2023 (2010).
[12] S. N. Majumdar and M. Vergassola, Phys. Rev. Lett. **102**, 060601 (2009).
[13] G. Ben Arous, A. Dembo, and A. Guionnet, Prob. Theory Related Fields **120**, 1 (2001).
[14] P. Vivo, S. N. Majumdar, and O. Bohigas, J. Phys. A **40**, 4317 (2007).
[15] M. Fridman, M. Nixon, N. Davidson, and A. A. Friesem, Opt. Lett. **35**, 1434 (2010).
[16] A. E. Siegman, *Lasers* (University Science Book, Mill Valley, California, 1986).
[17] V. Eckhouse, M. Fridman, N. Davidson, and A. A. Friesem, Phys. Rev. Lett. **100**, 024102 (2008).
[18] W. Chang, T. Wu, H. G. Winful, and A. Galvanauskas, Opt. Express **18**, 9634 (2010).
[19] A. Edelman and N. R. Rao, *Random Matrix Theory* (Cambridge University Press, 2005).
[20] M. Fridman, M. Nixon, E. Ronen, A. A. Friesem, and N. Davidson, Opt. Lett. **35**, 526 (2010).
[21] M. Khajavikhan and J. R. Leger, IEEE J. Quant. Electron. **15**, 281 (2009).
[22] M. Fridman, V. Eckhouse, N. Davidson, and A. A. Friesem, Opt. Lett. **32**, 790 (2007).
[23] S. J. August, T. Y. Fan, and A. Sanchez, Opt. Lett. **29**, 474 (2004).
[24] A. Shirakawa, K. Matsuo, and K. Ueda, Proc. SPIE **5662**, 482 (2004).
[25] E. J. Bochove and S. A. Shakir, IEEE J. Sel. Top. Quantum Electron. **15**, 320 (2009).
[26] S. H. Strogatz, Nature (London) **410**, 268 (2001).
[27] M. Fridman, R. Pugatch, M. Nixon, A. A. Friesem, and N. Davidson, e-print arXiv:1012.1292v1.

Preface

One of the first subjects in mathematics to attract my attention was integral equations; yet this book appears after a score of others. Why is this? It is because the writing of a book on integral equations is a rather difficult task, a task for which many years of meditation are necessary.

In fact, such a book must satisfy two requirements which are not easily reconciled. In order to facilitate theoretical applications to existence proofs it must present the main results of the theory with adequate generality and in accordance with modern standards of mathematical rigor. On the other hand, it must not be written so abstractly as to repel the physicist, engineer, and technician who certainly need and deserve this mathematical tool.

Have I succeeded in satisfying both requirements? Only the reader can decide. I can only hope that, if I have not always been successful in simplifying difficult matters, at least I shall not be found guilty of artificially complicating simple matters, a phenomenon which sometimes occurs in mathematical writing.

In the attempt to reconcile generality with simplicity, I was greatly helped by an idea put forward by my friend, Professor M. Picone.* Although already used by E. Schmidt, one of the founders of the theory of integral equations, this idea is still little known. By means of Neumann's series, it allows one to pass easily from an integral equation with a 'degenerate' kernel to one with a general kernel.

Here and there, especially in the last chapter, the specialist will find a few new things, or some old ones in a new form, e.g. the theory of Volterra integral equations in the L_2-space instead of the space of continuous functions. But, in general, I have avoided modifying material which has already reached a traditional, satisfactory systematization. I believe, moreover, that a book of this character should consider almost exclusively matters and methods which are already well established within the framework of analysis.

* Picone, M., *Appunti di analisi superiore,* Rondinella, Napoli, 1940.

$y = (1-t^2)/(1+t^2)$ we have

$$\mathscr{T}_x[(1-y^2)^{-\frac{1}{2}}] = \frac{2}{\pi}\int_0^{*\infty} \frac{dt}{(1-x)-(1+x)t^2} = 0 \quad (-1 < x < 1), \tag{12}$$

and consequently also

$$\mathscr{T}_x[(1-y^2)^{\frac{1}{2}}] = \frac{1}{\pi}\int_{-1}^{*1} \frac{(1-x^2)-(y^2-x^2)}{\sqrt{(1-y^2)}(y-x)}\,dy = -\frac{1}{\pi}\int_{-1}^{1} \frac{x+y}{\sqrt{(1-y^2)}}\,dy = -x. \tag{13}$$

Successively we apply the convolution theorem (5) to the pair of functions $\phi_1(x) = \sqrt{(1-x^2)}, \quad \phi_2(x) = \phi(x),$

which is certainly correct because the function $\phi_1(x)$, being bounded, belongs to the class $L^{p'}$ with any large p'. We have thus (almost everywhere)

$$\mathscr{T}_x[-y\phi(y)+\sqrt{(1-y^2)}f(y)] = -xf(x)-\sqrt{(1-x^2)}\phi(x).$$

But, on the other hand,

$$\mathscr{T}_x[y\,\phi(y)] = \frac{1}{\pi}\int_{-1}^{*1} \frac{y-x+x}{y-x}\phi(y)\,dy = x\mathscr{T}_x[\phi(y)]+\frac{1}{\pi}\int_{-1}^{1}\phi(y)\,dy.$$

Hence

$$\sqrt{(1-x^2)}\phi(x) = x\{\mathscr{T}_x[\phi(y)]-f(x)\}-\mathscr{T}_x[\sqrt{(1-y^2)}f(y)]+\frac{1}{\pi}\int_{-1}^{1}\phi(y)\,dy$$

$$= -\mathscr{T}_x[\sqrt{(1-y^2)}f(y)]+\frac{1}{\pi}\int_{-1}^{1}\phi(y)\,dy,$$

and we obtain

$$\phi(x) = -\frac{1}{\sqrt{(1-x^2)}}\mathscr{T}_x[\sqrt{(1-y^2)}f(y)]+\frac{C}{\sqrt{(1-x^2)}}$$

$$= -\frac{1}{\pi}\int_{-1}^{*1} \frac{\sqrt{(1-y^2)}f(y)}{\sqrt{(1-x^2)}(y-x)}\,dy+\frac{C}{\sqrt{(1-x^2)}}, \tag{14}$$

where, considering (12), the constant

$$C = \frac{1}{\pi}\int_{-1}^{1}\phi(y)\,dy \tag{15}$$

assumes the character of an arbitrary constant.

5. The precise significance of the previous result is naturally the following: *If the given equation has a solution of the class L^p ($p > 1$), then this solution must necessarily have the form* (14).

On the Spectra of Gaussian Matrices

Eric Kostlan
Department of Mathematics
University of Hawaii
Honolulu, Hawaii 96822

Submitted by David H. Carlson

ABSTRACT

We give a simple characterization of the moduli of the eigenvalues of a complex Gaussian matrix in terms of χ^2 distributions. We also show that the spectral radius of a $k \times k$ complex Gaussian matrix is stochastically smaller than the norm of a $k \times (k+1)$ real Gaussian matrix.

INTRODUCTION

Theorem 1.1 below gives a simple characterization of the moduli of the eigenvalues of a $k \times k$ complex Gaussian matrix in terms of χ^2 distributions. It states that the squared moduli of the eigenvalues behave like independent χ^2_{2k} distributions as i runs from one to k. The argument is similar to that of Ginibre [3], but the emphasis there is on the spectral radius. Theorem 2.2 gives a relationship between the distribution of the spectral radius of a $k \times k$ complex Gaussian matrix, the norm of a $k \times (k+1)$ real Gaussian matrix, and the χ^2_{2k} distribution. In particular, we establish a stochastic ordering for these three random variables. We begin with basic definitions and notation.

DEFINITION. A real Gaussian matrix is a matrix whose elements are independent standard Gaussian variables. A complex Gaussian matrix is a matrix whose real and imaginary parts are independent real Gaussian matrices.

NOTATION. $M^{(1)}_{k,n}$ will denote a $k \times n$ real Gaussian matrix. $M^{(2)}_{k,n}$ will denote a $k \times n$ complex Gaussian matrix. We will assume that $k \leqslant n$.

655 Avenue of the Americas, New York, NY 10010 0024-3795/92/$5.00

NOTATION. For any matrix M, $\| M \|_2$ will denote the operator norm of M with respect to the Euclidean norm. For any square matrix M, $\sigma(M)$ will denote the spectral radius of M, and per M will denote the permanent of M.

NOTATION. $\{X_i\}$ will denote independent nonnegative random variables such that X_i^2 has a χ_i^2 distribution.

1. GAUSSIAN MATRICES AND X^2 DISTRIBUTIONS

THEOREM 1.1. *The collection of moduli of the eigenvalues of $M_{k,k}^{(2)}$ has the same distribution as the collection of random variables $\{X_{2i}\}_{i=1,\cdots,k}$.*

Theorem 1.1 will follow immediately from Lemma 1.4 and Lemma 1.5. From this theorem we have the immediate

COROLLARY 1.2. $\text{Prob}[\sigma(M_{k,k}^{(2)}) > z] = \text{Prob}[\max\{X_{2i}\}_{i=1,k} > z]$. ■

For a discussion of $\sigma(M_{k,k}^{(1)})$, see Geman [2]. We will also make use of an analog of Corollary 1.2:

THEOREM 1.3. $\text{Prob}[\| M_{k,n}^{(\beta)} \|_2 > z] \geqslant \text{Prob}[\max\{X_{\beta(n+k-2i+1)}\}_{i=1,\cdots,k} > z]$.

Proof. This follow from inspection of the columns of the semidiagonalization of Gaussian matrices discussed in Silverstein [5]. Silverstein only proves the real case, but as mentioned by Edelman [1], his argument can be generalized. ■

LEMMA 1.4. *Let $r_1 \geqslant \cdots \geqslant r_k$ be the moduli of the eigenvalues of $M_{k,k}^{(2)}$. Then the joint density of $(r_i)_{i=1,\ldots,k}$ is given by*

$$\bar{B}_k \operatorname{per}\left[r_i^{2j-1}\right]_{i,j=1,\ldots,k} \exp\left[-\frac{1}{2}\sum_{i=1}^{k} r_i^2\right], \qquad \text{where} \quad \bar{B}_k = 2^k \prod_{j=1}^{k} \Gamma(j)^{-1}.$$

Proof. Let $\lambda_1, \cdots, \lambda_k$ be the eigenvalues of $M_{k,k}^{(2)}$, $|\lambda_1| \geqslant \cdots \geqslant |\lambda_k|$. Then the joint density of $(\lambda_i)_{i=1,\ldots,k}$ is given by

$$B_k \prod_{i<j} |\lambda_i - \lambda_j|^2 \exp\left[-\frac{1}{2}\sum_{i=1}^{k} |\lambda_i|^2\right], \qquad \text{where} \quad B_k = \pi^{-k} \prod_{j=1}^{k} \Gamma(j)^{-1}$$

—see Ginibre [3] for a proof and discussion. The quantity $\prod_{i<j} |\lambda_i - \lambda_j|^2$ is the squared modulus of the Vandermonde determinant:

$$\prod_{i<j} |\lambda_i - \lambda_j|^2 = \left| \sum_{\sigma \in S_k} (-1)^{\operatorname{sign}(\sigma)} \prod_{i=1}^{k} \lambda_i^{\sigma(i)-1} \right|^2,$$

where S_k denotes the permutation group on k symbols. Write $\lambda_i = r_i e^{i\theta_i}$. If $\sigma(j) \neq \sigma'(j)$ for some j, then

$$\int_0^{2\pi} \left(\prod_{i=1}^{k} r_i^{\sigma(i)-1} e^{i(\sigma(i)-1)\theta_i} \right) \overline{\left(\prod_{i=1}^{k} r_i^{\sigma'(i)-1} e^{i(\sigma'(i)-1)\theta_i} \right)} \, d\theta_j = 0.$$

Thus

$$\int_0^{2\pi} \cdots \int_0^{2\pi} \prod_{i<j} |\lambda_i - \lambda_j|^2 \, d\theta_1 \cdots d\theta_k = (2\pi)^k \sum_{\sigma \in S_k} \prod_{i=1}^{k} r_i^{2\sigma(i)-2}$$

$$= (2\pi)^k \operatorname{per}\left[r_i^{2j-2} \right]_{i,j=1,\ldots,k}.$$

Multiplying this by

$$\left(\prod_{i=1}^{k} r_i \right) \exp\left[-\frac{1}{2} \sum_{i=1}^{k} r_i^2 \right]$$

establishes the lemma. ∎

LEMMA 1.5. *Assume we are given an ordered k-tuplet of independent random variables* $(A_i)_{i=1,\ldots,k}$, *with corresponding densities* $(\rho_i)_{i=1,\ldots,k}$. *Define a new k-tuplet of random variables,* $(B_i)_{i=1,\ldots,k}$, *as a random permutation of the* (A_i), *each permutation considered equal in probability. Then the joint density of the random vector* $(B_i)_{i=1,\ldots,k}$ *is given by* $(1/k!)$ $\operatorname{per}[\rho_i(B_j)]_{i,j=1,\ldots,k}$. ∎

2. BARGMANN-MONTGOMERY-VON NEUMANN TYPE ESTIMATES

LEMMA 2.1.

$$\operatorname{Prob}\left[X_{\beta(n+k-1)} > z \right] \leqslant \operatorname{Prob}\left[\|M_{k,n}^{(\beta)}\|_2 > z \right]$$

$$\leqslant \frac{\Gamma(\beta/2)\Gamma(\beta(n+k-1)/2)}{\Gamma(\beta k/2)\Gamma(\beta n/2)} \operatorname{Prob}\left[X_{\beta(n+k-1)} > z \right].$$

Furthermore the right hand side is asymptotic to equality as $z \to \infty$.

It follows that this bound is optimal among all bounds of the form

$$C_1 \operatorname{Prob}\left[X_j > z \right] \leqslant \operatorname{Prob}\left[\| \mathrm{M}_{k,n}^{(\beta)} \|_2 > z \right] \leqslant C_2 \operatorname{Prob}\left[X_j > z \right],$$

where C_1, C_2, and j depend on n, k, and β, but not on z.

Proof. The left hand inequality follows immediately from theorem 1.3. The proof of the right hand inequality can be found in Goldstine and von Neumann [4, II.8.2]. Goldstine and von Neumann restrict their attention to the real square Gaussian matrices, but the argument can be generalized. See Edelman [1] for a discussion. ■

THEOREM 2.2.

$$\begin{aligned} \operatorname{Prob}\left[X_{2k} > z \right] &\leqslant \operatorname{Prob}\left[\sigma\left(\mathrm{M}_{k,k}^{(2)} \right) > z \right] \\ &\leqslant \operatorname{Prob}\left[\| \mathrm{M}_{k,k+1}^{(1)} \|_2 > z \right] \leqslant 2^{k-1} \operatorname{Prob}\left[X_{2k} > z \right]. \end{aligned}$$

Furthermore the left and right hand inequalities are asymptotic to equality as $z \to \infty$.

Proof. The left hand inequality follows from Corollary 1.2. It can be seen to by asymptotic by inspection of the density given in Lemma 1.4. The central inequality follows from Corollary 1.2 and Theorem 1.3. The right hand inequality is a special case of Lemma 2.1. ■

REFERENCES

1 A. Edelman, Eigenvalues and condition numbers of random matrices, *SIAM J. Matrix Anal. Appl.* 9:543–560 (1988).

2 S. Geman, The spectral radius of large random matrices, *Ann. Probab.* 14:1318–1328 (1986).

3 J. Ginibre, Statistical ensembles of complex, quaternion, and real matrices, *J. Math. Phys.* 6:440–449 (1965).

4 H. Goldstine and J. von Neumann, Numerical inverting of matrices of high order, in J. von Neumann, *Collected Works*, Vol. V, Pergamon, Oxford, 1963.

5 J. W. Silverstein, The smallest eigenvalue of a large dimensional Wishart matrix, *Ann. Probab.* 13:1364–1368 (1985).

Received 8 October 1990; final manuscript accepted 26 June 1991

J Stat Phys (2014) 154:466–490
DOI 10.1007/s10955-013-0838-1

Topology Trivialization and Large Deviations for the Minimum in the Simplest Random Optimization

Yan V. Fyodorov · Pierre Le Doussal

Received: 29 March 2013 / Accepted: 19 August 2013 / Published online: 10 September 2013

Abstract Finding the global minimum of a cost function given by the sum of a quadratic and a linear form in N real variables over $(N-1)$-dimensional sphere is one of the simplest, yet paradigmatic problems in Optimization Theory known as the "trust region subproblem" or "constraint least square problem". When both terms in the cost function are random this amounts to studying the ground state energy of the simplest spherical spin glass in a random magnetic field. We first identify and study two distinct large-N scaling regimes in which the linear term (magnetic field) leads to a gradual topology trivialization, i.e. reduction in the total number $\mathcal{N}_{tot}$ of critical (stationary) points in the cost function landscape. In the first regime $\mathcal{N}_{tot}$ remains of the order N and the cost function (energy) has generically two almost degenerate minima with the Tracy-Widom (TW) statistics. In the second regime the number of critical points is of the order of unity with a finite probability for a single minimum. In that case the mean total number of extrema (minima and maxima) of the cost function is given by the Laplace transform of the TW density, and the distribution of the global minimum energy is expected to take a universal scaling form generalizing the TW law. Though the full form of that distribution is not yet known to us, one of its far tails can be inferred from the large deviation theory for the global minimum. In the rest of the paper we show how to use the replica method to obtain the probability density of the minimum energy in the large-deviation approximation by finding both the rate function and the leading pre-exponential factor.

Keywords Random matrices · Random optimization · Random landscapes · Large deviations · Spin glasses · Replica method · Tracy-Widom distribution

Y.V. Fyodorov (✉)
School of Mathematical Sciences, Queen Mary University of London, London E1 4NS, UK
e-mail: Y.Fyodorov@qmul.ac.uk

P. Le Doussal
CNRS-Laboratoire de Physique Théorique de l'Ecole Normale Supérieure, 24 rue Lhomond, 75231 Paris Cedex, France
e-mail: pledoussal@yahoo.de

Equivalence principle

A few weeks ago I was lucky enough to be present at a lecture on statistical physics by Satya Majumdar, of the CNRS, University of Paris-Sud. Contrary to prevailing norms, Majumdar didn't use a laptop, and never showed a single PowerPoint slide. He wrote out words and equations with chalk on a blackboard. I'm not sure I've ever learned so much in only 30 minutes.

Majumdar started with some history about the growth of bacterial colonies. Seed a new colony on the surface of a nutrient medium, and it will grow into a vaguely circular blob, yet with an outer edge that is rough and gets rougher with time. Back in 1961, Murray Eden tried to explain the origin of this roughness, using a simple, linear mathematical model for diffusion driven by random noise. That model didn't work quantitatively.

Yet Eden helped kick off a study of irregular surfaces, growth processes and interfaces, which continues today. Surprising progress over the past two decades, Majumdar suggested, has researchers thinking they're just about to discover something truly profound. Unexpected links keep turning up between problems with no obvious connection.

In 1986, Mehran Kardar, Giorgio Parisi and Yi-Cheng Zhang modified Eden's model by including the lowest order nonlinear term. This model — known as the KPZ equation — does accurately describe how the irregular fluctuations grow in both space and time. Specifically, it predicts two exponents detailing how the mean square size of the fluctuations grows with time or when considering increasingly larger regions along the front.

If KPZ applied only to bacteria, it would be of marginal importance. But in the 1980s, as Majumdar recounted, in experiments and simulations physicists discovered that the KPZ exponents also fit lots of other irregular growth patterns arising in models of solid surface growth or in the way polymers orient themselves over disordered lattices, as well as in interface fluctuations of the bacterial type. To a large degree, KPZ seemed to capture a universal pattern in the emergence of fluctuations and roughness during irregular growth.

But how 'universal' is universal? As Majumdar stressed, this KPZ 'universality' referred only to the two exponents associated with the width (or second moment) of the distribution of fluctuations." It was unknown if the universality might run deeper — to the entire distribution of fluctuations — or might only be approximate.

Why does this Tracy–Widom distribution pop up in so many seemingly unrelated problems?

That was the end of the first part of the talk. Majumdar then turned to something very different: random matrices.

Imagine an $N \times N$ matrix with the entries being random numbers taken from a Gaussian distribution, and ask: what is the distribution of the largest eigenvalue of such a matrix? Random matrices were first introduced into physics by Eugene Wigner, and their study has found an extremely wide range of applications. In 1993, Majumdar noted, Craig Tracy and Harold Widom made a major breakthrough by calculating exactly the probability distribution of the largest eigenvalue in the large N limit. This eigenvalue has mean value $\sqrt{(2N)}$, and fluctuates over a range of width $N^{-1/6}$; the precise shape of the distribution is now called the Tracy–Widom distribution.

So what? Well, Majumdar went on to another famous mathematical problem — the Ulam problem, named after mathematician Stanislaw Ulam. Consider the $N!$ permutations of the first N integers $\{1, 2, 3, ..., N\}$. For each permutation, list all the possible increasing subsequences and then find the longest one. For $N = 5$, for example, the permutation $\{1, 3, 4, 2, 5\}$ has increasing subsequences such as $\{1, 5\}$, $\{1, 3, 4\}$ and $\{1, 3, 4, 5\}$, with the latter being the longest. The Ulam problem is to determine, for any N, and assuming that all $N!$ permutations are equally probable, the distribution of the length l_N of the longest increasing subsequence.

Ulam himself originally found that the average of l_N is proportional to $\sqrt{N}$ for large N. But l_N fluctuates about this mean. In 1999, mathematicians Jinho Baik, Percy Deift and Kurt Johansson derived the full distribution for large N, finding it to be $2\sqrt{N} + N^{1/6}\chi$, with χ being a fixed universal function. The surprise — the function turned out, again, to be the Tracy–Widom distribution, just as for random matrices.

Majumdar now moved to the punchline. Starting around the year 2000, several physicists and mathematicians discovered how to make an exact mapping between variants of the Ulam problem and models of the KPZ type, showing that these problems are entirely equivalent. Hence, there turns out to be an unexpected link between the Tracy–Widom distribution of random matrix theories and the physics of irregular growth. It is now known that a number of discrete models of the KPZ universality class follow the exact Tracy–Widom distribution, as does the continuous KPZ equation itself.

So, that open question about KPZ universality is no longer open — the universality it describes for a range of irregular growth processes indeed holds for the entire probability distribution, not only for the second moment. A beautiful experiment carried out in 2010 by Kazumasa Takeuchi and Masaki Sano made a precise measurement of the fluctuations during the irregular growth of drops of a liquid crystal and found precisely the Tracy–Widom distribution.

All of which leads to a satisfying theoretical unification — and also a puzzle. There does seem to be a deep universal connection between many different processes of the KPZ type. Strangely, it is also shared with many other things such as random matrices and the distribution of sub-sequences within longer sequences. What's going on? Why does this Tracy–Widom distribution pop up in so many seemingly unrelated problems?

Majumdar ended his talk here, suggesting that something enormously tantalizing lies just beyond our current view. Several recent studies (that he mentioned to me after the talk) have found signs of a peculiar 'third-order' phase transition lurking within all of these problems. This in turn appears to be closely linked to another generic phase transition — the Gross–Witten–Wadia transition — known from lattice gauge theories of quantum chromodynamics. But this is still conjecture.

Surprising and fascinating. I only wish the lecture could have lasted another few hours. ❐

MARK BUCHANAN